IISN0379-301X

UNIVERSITE LIBRE DE BRUXELLES - VRIJE UNIVERSITEIT BRUSSEL

INTER-UNIVERSITY INSTITUTE FOR HIGH ENERGIES

NEUTRAL STRANGE PARTICLE PRODUCTION IN ANTINEUTRINO-NEON CHARGED CURRENT INTERACTIONS

WA59 Collaboration

Universities of Brussels (ULB-VUB)
Pleinlaan, 2
1050 Brussels

September 1991
IIHE 91.03

PREPRINT
28 August 1991

Neutral Strange Particle Production in Antineutrino–Neon Charged Current Interactions

WA59 COLLABORATION

S. Willocq[3‡], P. Marage[3], M. Aderholz[6], P. Allport[8*], J.P. Baton[9], M. Berggren[10], E.F. Clayton[5], A.M. Cooper–Sarkar[8], O. Erriquez[1], P.J.W. Faulkner[2], J. Guy[8], P.O. Hulth[10], G.T. Jones[2], M.M. Mobayyen[5], D.R.O. Morrison[4], M. Neveu[9], S. O'Neale[2], J. Sacton[3], R.A. Sansum[11], K. Varvell[2], W. Venus[8], J. Wells[7], W. Wittek[6]

1 Dipartimento di Fisica dell'Università e Sezione INFN, I–70126 Bari, Italy.
2 University of Birmingham, Birmingham B15 2TT, UK.
3 Inter-University Institute for High Energies, ULB–VUB, B–1050 Brussels, Belgium.
4 CERN, CH–1211 Geneva 23, Switzerland.
5 Imperial College of Science and Technology, London, SW7 2AZ, UK.
6 Max-Planck-Institut für Physik und Astrophysik, W–8000 München 40, Germany.
7 Department of Nuclear Physics, Oxford, OX1 3RH, UK.
8 Rutherford Appleton Laboratory, Chilton, Didcot, OX11 0QX, UK.
9 DPhPE, Centre d'Etudes Nucléaires, Saclay, F–91191 Gif sur Yvette, France.
10 Institute of Physics, University of Stockholm, S–11346 Stockholm, Sweden.
11 Department of Physics and Astronomy, University College London, London WC1E 6BT, UK.

‡ Now at Tufts University, Medford, USA.
* Now at Cavendish Laboratory, Cambridge, UK.

Abstract

Neutral strange particle production in $\overline{\nu}$ Ne charged current interactions is studied using the bubble chamber BEBC, exposed to the CERN SPS antineutrino wide band beam. From a sample of 1191 neutral strange particles, the inclusive production rates are determined to be $(15.7 \pm 0.8)\%$ for $K^{0'}$ mesons , $(8.2 \pm 0.5)\%$ for Λ , $(0.4 \pm 0.2)\%$ for $\overline{\Lambda}$ and $(0.6 \pm 0.3)\%$ for Σ^0 hyperons. The inclusive production properties of K^0 mesons and Λ hyperons are investigated. The Λ hyperons are found to be polarized in the production plane.

1 — Introduction

The production of neutral strange particles in high energy neutrino and antineutrino interactions has been studied extensively.[1−14] It is generally considered that in the case of $\overline{\nu}$ charged current interactions strange particles are produced mainly by the following mechanisms (see Fig. 1) :

(a) associated $s\overline{s}$ pair production in the hadronization process,

(b) direct charm production on the strange sea ($\overline{s} \rightarrow \overline{c}$ transition), with an s quark as spectator and possibly an $\overline{s}$ quark from the Cabbibo-favoured decay of the $\overline{c}$ quark.

(c) Cabbibo-suppressed direct production of strange quarks ($u \rightarrow s$ transition).

Mechanisms (a) and (b) give rise to an even number of strange particles, whereas mechanism (c) produces single strange particles.

Neutral strange particles are quite easily and reliably identified in large bubble chambers, in contrast to most other hadrons. Therefore, they provide an excellent testing ground for the ideas of the quark-parton model as well as for hadronization models.

In this paper, we present results based on a sample of 1191 neutral strange particles produced in 13858 antineutrino charged current interactions (with muon momentum greater than 5 GeV/c) from an exposure of BEBC to the CERN SPS antineutrino wide band beam.

In Section 2, the experimental conditions and selection criteria of the event sample are presented. The inclusive production rates of neutral strange particles are extracted in Section 3. The differential rates for K^0 and Λ production and the single particle distributions are discussed in Sections 4 and 5. Λ polarization is investigated in Section 6. Finally, Section 7 summarizes the results.

2 — Experimental Procedure

The Big European Bubble Chamber (BEBC) was filled with a heavy Ne-H_2 mixture (75 mole % neon) and equipped with an External Muon Identifier (EMI) consisting of two planes of multiwire proportional chambers. It was exposed to the wide band antineutrino beam produced by 400 GeV protons from the CERN Super Proton Synchrotron (SPS).

For the present analysis, a sample of 51750 frames was carefully scanned for interactions induced by (anti)neutrinos. The events were subsequently measured and reconstructed using the standard CERN-HYDRA program chain. Details about the scanning and measurement procedures can be found in references 15 and 16. The events were required to be inside a 17 m^3 fiducial volume and to have an identified muon of positive charge with momentum greater than 5 GeV/c. The muons were identified using the EMI, with an 85% efficiency for momenta around 5 GeV/c and about 99 % for momenta larger than 10 GeV/c. If two or more muons were identified in the same event, the muon associated with the incoming (anti)neutrino was taken to be the one with the greatest value of the product $(p^\mu . p^\mu_T)$, where p^μ is the total muon momentum and p^μ_T is the muon momentum transverse to the beam direction.

Among the charged current events, 43 were too confused to be fully measured and were rejected for the present analysis, as were 32 events with an uncertainty on the total visible momentum or on the muon momentum greater than 30%. These rejected events do not contain abnormally large numbers of neutral strange particles. As a result, 13858 antineutrino charged current interactions were selected.

Neutral strange particles were detected via their decays into pairs of hadrons of opposite charge ("V^0"): $K^0 \to \pi^+\pi^-$, $\Lambda \to p\ \pi^-$ and $\overline{\Lambda} \to \overline{p}\ \pi^+$. By "K^0" we denote both K^0 and $\overline{K^0}$ mesons since no distinction between them is possible in the present experiment. All V^0 possibly produced at the antineutrino interaction were measured and constrained to fit the above decay hypotheses to all physical origins. The fit probability was then required to be greater than 10^{-4} for the fit to be retained. When more than one physical origin was acceptable, the fit to the primary vertex was selected if its probability was greater than 1 % or if it had the highest probability. There were 1191 V^0 with acceptable fits to the primary vertex.*

In order to ensure good V^0 detection and measurement efficiencies, the V^0 vertices were required to be at a distance greater than 1 cm from the primary vertex and at least 25 cm in front of the bubble chamber wall. The cut at 1 cm was chosen empirically from the distribution of the distance between the primary and V^0 vertices. Furthermore, the V^0 lifetime was required to be smaller than 6 times the corresponding mean lifetime, in an attempt to remove the V^0 which have an acceptable fit to the primary vertex but which more likely originate from a secondary vertex, downstream from the antineutrino interaction.

In this analysis, particular attention was paid to the choice of the minimum accepted value for the χ^2-probability of the fits. Indeed, backgrounds of several types are expected to be concentrated at low probability. In particular, neutron or K^0_L interactions giving

---

* In the case of γ/V^0 ambiguity, both V^0 and γ fits were attempted. If an acceptable fit was obtained for the γ hypothesis, it was always selected.

rise to two particles of opposite charge, and genuine K^0 or Λ originating from a secondary vertex, can occasionally give an acceptable fit to the primary vertex. On the other hand, it was observed that the V^0 with a fit probability lower than 5% have an average momentum significantly larger than the V^0 with higher fit probabilities. A value of 0.5% for the lowest acceptable fit probability has been chosen, as a compromise between efficient background rejection and reliable unbiased selection.

The effect of the selection criteria is summarized in Table 1. Among the 1020 V^0 surviving the above cuts, 804 are unambiguous, viz. 463 K^0, 333 Λ and 8 $\overline{\Lambda}$, and 216 are ambiguous, viz. 163 K^0/Λ, 50 $K^0/\overline{\Lambda}$, 2 $\Lambda/\overline{\Lambda}$ and 1 $K^0/\Lambda/\overline{\Lambda}$ (see Table 2).

The ambiguities between the different V^0 interpretations were resolved by using the distribution of the cosine of the angle (θ^*) between the positive decay track and the V^0 line of flight (Lorentz boost direction) in the V^0 rest frame. For K^0, this distribution is expected to be flat since the decay is isotropic in the K^0 rest frame (this would not be true for polarized Λ or $\overline{\Lambda}$). The cos θ^* distribution for all K^0 fits is shown in Fig. 2a. It is observed that the ambiguous V^0 do not contribute significantly to the central region defined as $|\cos \theta^*| < 0.6$. The mean number of K^0 fits per bin in this region can therefore be extrapolated to the whole range of cos θ^* (dashed line in Fig. 2a) and the fraction of true K^0 among the ambiguous V^0 can be determined. As a result, the number of genuine K^0 expected among the K^0/Λ fits is 25 ± 9, whereas it is 33 ± 9 among the $K^0/\overline{\Lambda}$ fits.* The systematic uncertainty on these numbers due to the choice of the central region is estimated to be ± 2. This gives the following numbers of neutral strange particles : 521 K^0, 474 Λ and 25 $\overline{\Lambda}$. Table 2 summarizes the results of the ambiguity resolution procedure.

The ambiguity resolution procedure only tells which fraction of the ambiguous V^0 have to be interpreted as K^0, Λ or $\overline{\Lambda}$. The actual resolution of the ambiguity for each V^0 is done on the basis of the ratio of fit probabilities, such as to reproduce the results of the above procedure. K^0/Λ ($K^0/\overline{\Lambda}$) ambiguities are resolved in favour of the K^0 hypothesis whenever the K^0 fit probability is greater than 1.95 (0.95) times the Λ ($\overline{\Lambda}$) fit probability; the Λ interpretation is chosen in the cases of $\Lambda/\overline{\Lambda}$ and $K^0/\Lambda/\overline{\Lambda}$ ambiguity.

A Monte Carlo study[17] of K^0/Λ and $K^0/\overline{\Lambda}$ ambiguities in BEBC indicates that the fit probability provides an efficient separation between the different mass hypotheses. In this case, possible contamination of the K^0 and Λ samples due to an erroneous interpretation of the ambiguities is small. In the Λ sample (474 Λ in total), the contamination would

---

* As expected, those two numbers are nearly equal since the decay of K^0 mesons into positive and negative pions is symmetric, thus simulating Λ and $\overline{\Lambda}$ equally.

not exceed 5% even if the resolution algorithm were to pick each of the 25 genuine K^0 appearing among the 163 K^0/Λ ambiguities. Similarly, in the K^0 sample, even if only the genuine Λ and $\overline{\Lambda}$ were selected, this would lead to a maximum contamination of 8% (25 Λ and 17 $\overline{\Lambda}$ on a total of 521 K^0). However, the contamination of the $\overline{\Lambda}$ sample could be large.

The cos θ^* distributions for K^0 and Λ , after the resolution of ambiguities, are shown in Figs. 2b and 2c. The lack of Λ with large cos θ^* suggests a possible loss of Λ with π^- of low momentum in the laboratory : such Λ are indeed difficult to find and to reconstruct. This is supported by the fact that only 2 out of 30 Λ with cos $\theta^* > 0.8$ have momentum < 1 GeV/c, whereas 141 out of 444 Λ with cos $\theta^* < 0.8$ have momentum < 1 GeV/c. The loss of Λ with momentum below 1 GeV/c is estimated by comparing the observed and simulated π^- momentum distributions for Λ in that momentum range (we used the observed Λ momentum distribution below 1 GeV/c to simulate Λ decays). This loss will be corrected hereafter by weighting appropriately the observed low momentum Λ . The Λ decay angular characteristics are studied in more detail in Section 6.

The unconstrained $\pi^+\pi^-$ and p π^- invariant masses for selected K^0 and Λ are displayed in Fig. 3. Fitting the distributions with Gaussians gave mass values of $m(K^0) = (497.5 \pm 0.7)$ MeV/c^2 and $m(\Lambda) = (1115.8 \pm 0.4)$ MeV/c^2, in agreement with the Particle Data Group values.[18]

The V^0 are weighted according to the probability of decay inside the allowed region; a region which is determined by the cuts on the distance from the primary vertex and from the bubble chamber wall, as well as by the lifetime cut. In addition, the V^0 are weighted according to their probability of interaction before decay. The combined V^0 scanning and kinematical fitting efficiency is estimated to be (96 ± 2)% from two independent V^0 scans and partial remeasurements. The average K^0 and Λ weights shown in Table 3 also take into account the branching fraction for neutral decay modes (including the undetected K^0_L component) and the loss of Λ with slow π^-. No correction is made for the γ/K^0 or γ/Λ ambiguities which are expected to be negligible.

A final test of the quality of the sample comes from the lifetime measurement (Fig. 4). The use of a maximum likelihood method[19] yields mean lifetimes of $(0.862 \pm 0.042) \times 10^{-10}$s for K^0_s and $(2.64 \pm 0.13) \times 10^{-10}$s for Λ , in good agreement with the P.D.G. values[18] (0.892 $\times 10^{-10}$ and 2.63 $\times 10^{-10}$ s respectively).

3 — Production Rates

For the purpose of calculating production rates, the observed number of V^0 is weighted as described above. Furthermore, the number of charged current interactions (with or without V^0) is corrected for scanning losses according to the charged and neutral particle multiplicities (see reference 16).

In order to be above the threshold for K^0 production, the total hadronic invariant mass squared W^2 is required to be greater than $(m_N + m_{K^0})^2$, where m_N is the nucleon mass. This cut reduces the number of V^0 to 1012, i.e. 518 K^0, 469 Λ and 25 $\overline{\Lambda}$. The total number of charged current events passing the cut is 12289, leading to corrected production rates* of (15.7 ± 0.8)% for K^0 , (8.2 ± 0.5)% for Λ and (0.4 ± 0.2)% for $\overline{\Lambda}$. The corresponding rates for $W^2 > 5$ GeV^2 are (18.4 ± 1.0)% for K^0 , (8.6 ± 0.5)% for Λ and (0.5 ± 0.2)% for $\overline{\Lambda}$.

Table 4 summarizes the most statistically significant results published on K^0 and Λ production rates in antineutrino charged current interactions. Comparison between these data is difficult due to the different experimental procedures, different cuts and different targets. For antineutrino energies averaging around 40 GeV, all K^0 production rates seem broadly consistent while the Λ rates vary from 4 to 8 %, with the lowest rates being obtained in $\overline{\nu}$ p interactions. For completeness, the most significant results in neutrino charged current interactions are also given in Table 4.

Table 5 presents the semi-inclusive production rates for single and multiple V^0 production channels. These rates are obtained by solving the complete set of equations relating the number of observed events in each channel to the true number of events from all contributing production channels, given the detection efficiencies. The ratio (R) between the rates for pair production and single production of neutral strange particles, defined as $\left(\frac{\# K^{-0}K^{-0} + \# K^{-0}\Lambda}{\# K^{-0} + \# \Lambda}\right)$, is 0.60 ± 0.12, a value consistent with most neutral strange particles being produced in association with another strange particle, either neutral or charged**.

---

[*] The systematic error corresponding to the uncertainties in the total weight and in the resolution of the ambiguities has been added to the statistical error in quadrature.

[**] If it is assumed that charged and neutral kaons are produced with equal probability and that $K^0\Lambda$ (or $K^+\Lambda$) pair production occurs at 0.5 to 1 times the rate of $K^0\overline{K^0}$ (or K^0K^- or $\overline{K^0}K^+$) pair production, then one expects the ratio R to be in the range 0.60 to 0.67 if all V^0 are due to associated production. No associated production would result in $R = 0$.

The study of the production of $\Sigma^0(\rightarrow \Lambda\gamma)$ hyperons is possible in this experiment, taking advantage of the good γ detection efficiency in the heavy Ne-H_2 mixture (density 0.71 g/cm^3 and radiation length 41.6 cm).

Fig. 5 shows the $\Lambda\gamma$ invariant mass distribution. A definite peak at the Σ^0 mass (1.193 GeV/c^2) is observed, where the mass resolution is 0.010 GeV/c^2. The background is determined by randomly combining each Λ with γ from other events with similar values of W^2 ; it is then normalized to the number of mass combinations outside the Σ^0 region (1.160 to 1.220 GeV/c^2) and fitted with a fifth order polynomial (curve in Fig. 5). As a result, the number of Σ^0 above background is estimated to be 22 ± 10.

In order to compute the Σ^0 production rate, the observed number has to be corrected for the γ detection and reconstruction efficiency $(65 \pm 1)\%$ (see reference 16), as well as for the overall Λ detection efficiency (see Table 3). The corrected number of Σ^0 is found to be 76 ± 34, leading to a production rate of $(0.6 \pm 0.3)\%$, while the ratio between Σ^0 and Λ production rates is found to be $(7.3 \pm 3.3)\%$. The only other measurement of the Σ^0 production rate comes from a neutrino experiment[14] in which the rate was estimated to be $(1.1 \pm 0.3)\%$.

Table 6 summarizes our measurements of the inclusive production rates of K^0 mesons, Λ , $\overline{\Lambda}$ and Σ^0 hyperons.

4 — Differential Rates

The production properties of K^0 mesons and Λ hyperons are studied as a function of various kinematical variables which characterize the interaction as a whole: the antineutrino energy E, the energy transfer $\nu = E - E^\mu$, the square of the 4-momentum transfer between the antineutrino and the target nucleon $Q^2 = 2E(E^\mu - p_L^\mu) - m_\mu^2$, the Bjorken variables $x = Q^2/(2m_N\nu)$ and $y = \nu/E$, and the total hadronic mass squared $W^2 = m_N^2 + 2m_N\nu - Q^2$. E is estimated from the momenta of all measured charged and neutral particles in the following way:

$$E = p_L^\mu + S \cdot f(S)$$

with $S = |\sum p_L^i|$, summing over all particles excluding the muon. The variables p_L^i and p_L^μ denote the longitudinal momentum of particle i and of the muon, with respect to the antineutrino direction. The function f corrects the visible momentum for the loss of neutral particles as determined by Monte Carlo[16].

Table 7 gives the average values of the kinematical variables distributions for the events containing K^0 or Λ and for the whole charged current sample with $W^2 > (m_N + m_{K^0})^2$. The differential production rates for K^0 and Λ particles as a function of E, ν, Q^2, x, y and W^2 are shown in Figs. 6 to 11.

Both K^0 and Λ production rates increase with increasing E, ν, Q^2, y and W^2 , the increase being stronger for the K^0 than for the Λ. The K^0 rate seems to level off at high values of E, ν, Q^2 and W^2 (Figs. 6, 7, 8 and 11) and to decrease at high y values (Fig. 10). The apparent lack of K^0 at high W^2 was also seen in some of the other experiments[9−11,14], including the one with the largest (neutrino) statistics. However, it is expected that the smearing due to measurement errors, particle misidentification and $\overline{\nu}$ energy estimation would produce such an effect. The possible loss of K^0 decaying inside high multiplicity hadronic or electromagnetic showers may also contribute.

Fig. 9 shows that both K^0 and Λ production rates are essentially independent of x. This is in contrast to the strong dependence observed by Ammosov et al[6], which was attributed to the contribution from charm production off the strange sea, at small values of x. However, it should be noted that a fraction as large as 45% [20] of all antineutrino charged current interactions takes place on the sea. The effect in x is thus not expected to be large. Allasia et al[11] report a decrease in the K^0 production rate with increasing x, while the Λ production rate is independent of x. This decrease in the K^0 rate cannot be very pronounced since they report average values of x for K^0 events (0.21 ± 0.02 for $\overline{\nu}$ n and 0.20 ± 0.02 for $\overline{\nu}$ p) close to those for all charged current events (0.18 ± 0.01 for $\overline{\nu}$ n and 0.23 ± 0.01 for $\overline{\nu}$ p).

The Λ production rate as a function of W^2 (Fig. 11) is essentially flat below ~ 15 GeV^2 and increases above that value. This rise could be attributed to a threshold effect for charm production. Indeed, the interactions off the strange sea are Cabbibo-suppressed below the charm threshold ($\overline{s} \rightarrow \overline{u}$ transitions). Above the threshold for charm production, the $\overline{s} \rightarrow \overline{c}$ transition is favoured and the remaining s quark may recombine with valence quarks to form a Λ hyperon. This threshold effect has no counterpart in ν interactions and is not observed in other experiments (see for example reference 14). The rise appears for both ambiguous and unambiguous Λ , thus it is not due to a contamination of the Λ sample by K^0.

To substantiate this interpretation, the V^0 production rates were examined as a function of W^2 for the events with total measured charge Q = 0 (Figs. 12a and 12c) and Q = 1 (Figs. 12b and 12d). About 90 % of the events with Q = 0 are interactions on neutrons whereas nearly 85 % of those with Q = 1 are interactions on protons. At low W^2 , the Λ production rate is higher for interactions on protons than it is for interactions on neutrons. In the case of interactions on proton valence quarks, a u quark is struck and the ud diquark left behind can then pick up a strange quark from the sea to form a Λ or Σ^0 hyperon (see Fig. 13a). On the other hand, in the case of interactions on neutron valence quarks, the dd diquark left behind has to break up to produce a Λ or Σ^0 (Fig. 13b). This explains why the opening of the charm production channels is expected to show up more prominently in $\overline{\nu}$ n than in $\overline{\nu}$ p interactions, as observed in Fig. 12.

Other variables were studied separately for events with W^2 below or above the observed threshold. Within the rather large statistical errors, no significant difference was observed.

The data reported by Allasia et al[11], obtained under similar experimental conditions (same $\overline{\nu}$ beam and bubble chamber), are compared with our data in Figs. 11 and 12. The Lund model predictions for deuterium, extracted from reference 11 (see also reference 12), are shown as well. It should be noted that different smearing conditions might affect the two data sets in slightly different ways. Good overall agreement between the Lund model predictions and our data is observed.

5 — Single Particle Distributions

The production properties of individual particles can be described as a function of:

i) the transverse momentum squared with respect to the direction of motion of the hadronic system, p_T^2;

ii) the fraction of the W boson energy carried in the laboratory system, $z = E_{V^0}/\nu$;

iii) the Feynman-x variable, x_F, approximated by $2p_L^*/W$, where p_L^* is the longitudinal momentum (with respect to the direction of motion of the hadronic system) in the hadronic center of mass system;

iv) the rapidity in the hadronic center of mass system, $y^* = \frac{1}{2}\ln[(E^* + p_L^*)/(E^* - p_L^*)]$, where E^* is the energy in the hadronic center of mass system.

In this section, a cut at $W^2 > 5$ GeV^2 is applied in order to decrease the influence of exclusive channels at low energy. The V^0 production properties are shown in Figs. 14 to 17 and summarized in Table 8*. As in the previous section, data from reference 11 for the

---

* It should be noted that the distributions shown here have not been corrected for the smearing due to measurement errors, particle misidentification and $\overline{\nu}$ energy estimation.

same W^2 have been superimposed for comparison.

The p_T^2 distributions for K^0 and Λ given in Fig. 14 were fitted by an expression of the form $A \cdot exp[Bp_T^2]$ for transverse momenta squared up to 0.5 $(\mathrm{GeV/c})^2$. The slope parameters were found to be $B = -4.93 \pm 0.46$ $(\mathrm{GeV/c})^{-2}$ and $B = -4.69 \pm 0.52$ $(\mathrm{GeV/c})^{-2}$ for K^0 and Λ respectively. Similar values have been obtained in previous neutrino and antineutrino experiments.

The z distributions are shown in Fig. 15. The mean is 0.25 ± 0.01 for K^0 and 0.22 ± 0.01 for Λ. There is an indication of a turnover at low z for the K^0 data. Such a behaviour was also observed in most other experiments although no turnover was observed by Bosetti et al[10] in a study performed at higher E and W^2.

The x_F-distribution for K^0 (Fig. 16) is a narrow distribution around zero while the Λ distribution is wider and mostly at $x_F < 0$. This can be characterized by the asymmetry parameter A defined as $(N_F - N_B)/(N_F + N_B)$, where N_F (N_B) is the number of particles moving forward (backward) in the hadronic center of mass system. The values obtained for K^0 and Λ are $A = 0.23 \pm 0.04$ and $A = -0.72 \pm 0.04$ respectively.

The rapidity distributions (Fig. 17) show features similar to the x_F-distributions, although the rapidity depends on both longitudinal and transverse momenta. The x_F and y^* distributions thus indicate that K^0 (Λ) production essentially occurs in the central (backward) region of the hadronic center of mass system. However, it is observed that 31 Λ (of which 18 are unambiguously identified) are produced in the forward region $y^* > 0.2$. 28 of these 31 Λ belong to events with $W^2 > 20$ GeV^2 , whereas only 17 of the 77 Λ with $-0.2 < y^* < 0.2$ belong to events with $W^2 > 20$ GeV^2 . There is thus a signal for Λ production in the forward region, with little background from K^0 . It is interesting to note that the $\overline{\Lambda}$ (also at high W^2) and forward Λ candidates found in this sample may be interpreted as evidence for baryon-antibaryon pair production.

Overall, the data and Lund model predictions extracted from reference 11 and displayed on the p_T^2, z and x_F distributions show features similar to our data.

6 — Λ Polarization

Λ polarization has been studied in several experiments[5,11,21]. Jones et al[21] observe polarization in the Λ production plane, defined by the $\hat{J}$ and $\hat{T}$ directions described below, whereas Ammosov et al[5] and Allasia et al[11] find polarizations transverse to the production plane, defined by the Λ and $\overline{\nu}$ directions in the laboratory, but with opposite signs.

Polarization is expected to occur in Λ production as a result of the space-time structure of the weak current. When the W boson interacts with a valence quark of left-handed helicity, the leftover diquark from the initially unpolarized nucleon is expected to retain a remnant polarization. This polarization may be transmitted to the strange baryon formed by picking up a strange quark from the (unpolarized) sea[22].

The angular distribution of the decay proton in the Λ rest frame can be written in the form

$$\frac{dN}{dcos\theta\ d\phi} = \frac{1}{4\pi}\ (1 + \alpha\ \vec{P}_\Lambda \cdot\ \hat{p}_p),$$

where the parameter $\alpha = 0.642 \pm 0.013$ (from reference 18), $\vec{P}_\Lambda$ is the polarization vector of the Λ and $\hat{p}_p$ is a unit vector in the direction of the decay proton. The angles θ and ϕ are the polar and azimuthal angles of the decay proton with respect to $\vec{P}_\Lambda$.

The axes in the Λ rest frame are defined as follows:

$$\hat{x}' = \hat{J}$$

$$\hat{y}' = \hat{J} \times \hat{T}\ /\ |\hat{J} \times \hat{T}|$$

$$\hat{z}' = \hat{x}' \times \hat{y}'$$

where $\hat{J}$ is a unit vector along the current (W boson) direction and $\hat{T}$ is a unit vector in the direction of the target nucleon (assumed to be initially at rest in the laboratory). These two directions define the production plane. It should be noted that this definition of the production plane agrees with that of reference 21, whereas it is different from the one of references 5 and 11.

The distributions of the cosine of the angle between the decay proton and the x', y' and z' axes are shown in Fig. 18. A fit to these distributions using the above expression gives the following values for the polarization $\vec{P}_\Lambda$: -0.56 ± 0.13 , -0.02 ± 0.13 and 0.08 ± 0.13 along the x', y' and z' axes respectively. A strong effect is observed in the direction opposite to the current (Fig. 18a), whereas no polarization is found perpendicular to the production plane (Fig. 18b) or along the z' axis (Fig. 18c). A systematic error of ± 0.02 on the above numbers is estimated taking into account the uncertainty in the resolution of K^0/Λ ambiguities and the correction for low momentum π^-. No correction is made for the γ/Λ ambiguity. The effect is definite for $x_F < 0$ and persists for a series of cuts on the kinematical variables (see Table 9).

These results confirm the observation by G.T. Jones et al[21] that the polarization component perpendicular to the Λ production plane is consistent with zero and that significant polarization is observed in the Λ production plane. As a check, the polarization analysis was repeated on the sample of unambiguous K^0. No significant polarization effect was found in that sample.

7 — Summary

The production of neutral strange particles in antineutrino charged current interactions has been studied in BEBC filled with a heavy Ne-H_2 mix. The total number of K^0, Λ and $\overline{\Lambda}$ passing the selection criteria is 518, 469 and 25 respectively for $p^\mu > 5$ GeV/c and $W^2 > (m_N + m_{K^0})^2$. The corresponding number of charged current events is 12289. The inclusive production rates are $(15.7 \pm 0.8)\%$ for K^0, $(8.2 \pm 0.5)\%$ for Λ, $(0.4 \pm 0.2)\%$ for $\overline{\Lambda}$ and $(0.6 \pm 0.3)\%$ for Σ^0 (included in the Λ rate).

It is found that both K^0 and Λ production rates increase with increasing E, ν, Q^2, y and W^2, the increase for the K^0 being stronger than for the Λ . An indication for a charm threshold effect is found in the Λ production rate as a function of W^2.

The production properties of K^0 and Λ have been studied as a function of p_T^2, z, x_F and y^*. The results indicate that most K^0 are produced centrally while most Λ are produced backward. These features are in qualitative agreement with the quark-parton model predictions.

Finally, the Λ hyperons are found to be polarized in the production plane while the polarization perpendicular to the production plane is consistent with zero.

Acknowledgements

We express our gratitude to the CERN staff for excellent beam conditions and bubble chamber operation and to the scanning and measuring staff in our institutions for their dedicated work.

REFERENCES

[1] H. Deden et al., Phys. Lett. 58B, 361 (1975).

[2] J.P. Berge et al., Phys. Rev. Lett. 36, 127 (1976).

[3] J.P. Berge et al., Phys. Rev. D18, 1359 (1978).

[4] O. Erriquez et al., Nucl. Phys. B140, 123 (1978).

[5] V.V. Ammosov et al., Nucl. Phys. B162, 205 (1980).

[6] V.V. Ammosov et al., Nucl. Phys. B177, 365 (1981).

[7] N.J. Baker et al., Phys. Rev. D24, 2779 (1981).

[8] R. Brock et al., Phys. Rev. D25, 1753 (1982).

[9] H. Grässler et al., Nucl. Phys. B194, 1 (1982).

[10] P. Bosetti et al., Nucl. Phys. B209, 29 (1982).

[11] D. Allasia et al., Nucl. Phys. B224, 1 (1983).).

[12] D. Allasia et al., Phys. Lett. 154B, 231 (1985). In this publication, the number of K^0 and Λ found in a sample of 13000 (8600) ν ($\overline{\nu}$) charged current events is not given. The rates reported in a previous publication[11] were similar for ν interactions but slightly different for $\overline{\nu}$ interactions: the K^0 production rate in $\overline{\nu}$n and $\overline{\nu}$p interactions was $(21.9 \pm 2.5)\%$ and $(22.2 \pm 1.8)\%$ respectively, whereas the Λ production rate was $(8.2 \pm 1.2)\%$ and $(7.0 \pm 0.8)\%$ respectively.

[13] V.V. Ammosov et al., Z. Phys. C30, 183 (1986).

[14] N.J. Baker et al., Phys. Rev. D34, 1251 (1986).

[15] K. Varvell et al., Z. Phys. C36, 1 (1987).

[16] W. Wittek et al., Z. Phys. C40, 231 (1988).

[17] V. Karimäki and Y.L. Petrovykh, CERN/EP/DHR 77–5.

[18] J.J. Hernandez et al. (Particle Data Group), Phys. Lett. B239, 1 (1990): Review of Particle Properties.

[19] W.T. Eadie et al.,*Statistical Methods in Experimental Physics*, North Holland, Amsterdam and London, 1971.

[20] This number can be extracted using the quark-parton model expressions for $\overline{\nu}$ n and $\overline{\nu}$ p cross sections, as well as the integrated fraction of momentum carried by quarks and antiquarks obtained in a recent study of structure functions by P.N. Harriman et al., Phys. Rev. D42, 798 (1990).

[21] G.T. Jones et al., Z. Phys. 28, 23 (1985).

[22] I.I.Y. Bigi, Nuovo Cimento 41A, 581 (1977).

TABLE 1 : Total number of V^0 originating from the primary vertex as a function of the successive selection criteria.

No cut	1191
$l > 1.0$ cm	1110
$d_{wall} > 25$ cm	1102
$t < 6\tau$	1074
$P > 0.5\%$	1020

TABLE 2 : Numbers of V^0 fits and their assignment to different mass hypotheses.

	K^0	K^0/Λ	$K^0/\overline{\Lambda}$	$K^0/\Lambda/\overline{\Lambda}$	Λ	$\Lambda/\overline{\Lambda}$	$\overline{\Lambda}$	Sum
K^0	463	25	33	—	—	—	—	521
Λ	—	138	—	1	333	2	—	474
$\overline{\Lambda}$	—	—	17	—	—	—	8	25
Sum	463	163	50	1	333	2	8	1020

TABLE 3 : Average weights and correction factors applied to K^0 and Λ (the average total weight also includes a $\sim 4\%$ correction for overall charged current event scanning efficiency).

	K^0	Λ
V^0 scanning and kinematical fitting eff.	1.042 ± 0.022	1.042 ± 0.022
Geometric detection efficiency	1.156 ± 0.008	1.170 ± 0.008
Interaction before decay	1.063 ± 0.004	1.072 ± 0.006
Neutral decay modes	2.915 ± 0.011	1.560 ± 0.012
Low momentum π^-	—	1.048 ± 0.021
Average total weight	3.876 ± 0.089	2.231 ± 0.072

TABLE 4 : Inclusive production rates for K^0 and Λ produced in $\overline{\nu}$ and ν charged current interactions. $< E_{CC} >$ is the average (anti)neutrino energy of the charged current event sample.

Reaction	Cuts (GeV)	$< E_{CC} >$ (GeV)	# K^0 observed	K^0 Rate (%)	# Λ observed	Λ Rate (%)
$\overline{\nu}$ Ne $^{\text{this exp.}}$	$p^\mu > 5, W > m_N + m_{K^0}$	40	518	15.7 ± 0.8	469	8.2 ± 0.5
$\overline{\nu}$ n [12]	$p^\mu > 4, W > \sqrt{5}$	~ 45		20.8 ± 2.0		7.6 ± 0.8
$\overline{\nu}$ p [12]	$p^\mu > 4, W > \sqrt{5}$	~ 45		18.4 ± 1.3		5.7 ± 0.6
$\overline{\nu}$ Ne [10]	$p^\mu > 5, W > 1.5$	81	64	21.9 ± 2.8	37	6.5 ± 1.2
$\overline{\nu}$ p [8]	$E > 5, W > 1.0$	~ 45	88	15.1 ± 3.2	46	4.5 ± 0.9
$\overline{\nu}$ Ne [6]	$p^\mu > 4, E > 10$	~ 45	350	16.4 ± 0.9	257	6.3 ± 0.4
ν Ne [14]	$p^\mu > 2, E > 10$	46	2279	16.8 ± 1.2	1843	6.5 ± 0.5
ν Freon [13]	$E > 3, W > 1.5$	10	82	7.1 ± 0.8	76	3.1 ± 0.4
ν n [12]	$p^\mu > 4, W > \sqrt{5}$	~ 60		20.5 ± 1.2		6.6 ± 0.7
ν p [12]	$p^\mu > 4, W > \sqrt{5}$	~ 60		17.4 ± 1.2		4.4 ± 0.5
ν Ne [10]	$p^\mu > 5, W > 1.5$	103	203	23.0 ± 1.7	98	5.7 ± 0.7
ν p [9]	$p^\mu > 3, E > 5, W > 1.5$	43	359	17.5 ± 0.9	180	4.5 ± 0.4

TABLE 5 : Semi-inclusive production rates for single and multiple V^0 final states. X represents any hadronic final state which does not contain K^0, Λ or $\overline{\Lambda}$. The numbers in the second column are the "true" numbers of events in each of the 9 channels obtained by solving the system of 9 equations. ($p^{\mu} > 5$ GeV/c and $W^2 > (m_N + m_{K^0})^2$)

Semi-inclusive channel	# Events observed	# Events (solution)	Rate (%)
$\bar{\nu}\ \mathrm{Ne} \rightarrow \mu^+\ \mathrm{K}^0\ X$	408	738 ± 159	5.8 ± 1.2
$\bar{\nu}\ \mathrm{Ne} \rightarrow \mu^+\ \Lambda\ X$	404	565 ± 77	4.4 ± 0.6
$\bar{\nu}\ \mathrm{Ne} \rightarrow \mu^+\ \overline{\Lambda}\ X$	19	14 ± 22	0.11 ± 0.17
$\bar{\nu}\ \mathrm{Ne} \rightarrow \mu^+\ \mathrm{K}^0\ \mathrm{K}^0\ X$	28	402 ± 84	3.1 ± 0.7
$\bar{\nu}\ \mathrm{Ne} \rightarrow \mu^+\ \mathrm{K}^0\ \Lambda\ X$	49	374 ± 81	2.9 ± 0.6
$\bar{\nu}\ \mathrm{Ne} \rightarrow \mu^+\ \mathrm{K}^0\ \overline{\Lambda}\ X$	3	25 ± 17	0.19 ± 0.13
$\bar{\nu}\ \mathrm{Ne} \rightarrow \mu^+\ \Lambda\ \Lambda\ X$	6	30 ± 12	0.23 ± 0.10
$\bar{\nu}\ \mathrm{Ne} \rightarrow \mu^+\ \Lambda\ \overline{\Lambda}\ X$	3	14 ± 10	0.11 ± 0.08
$\bar{\nu}\ \mathrm{Ne} \rightarrow \mu^+\ \mathrm{K}^0\ \mathrm{K}^0\ \Lambda\ X$	1	34 ± 34	0.26 ± 0.26

TABLE 6 : Inclusive production rates for K^0 , Λ , $\overline{\Lambda}$ and Σ^0 . The corrected number of charged current events is 12812, after taking the scanning efficiency into account. ($p^{\mu} > 5$ GeV/c and $W^2 > (m_N + m_{K^0})^2$)

	Number of V^0 observed	Number of V^0 corrected	Rate (%)
K^0	518	2008 ± 107	15.7 ± 0.8
Λ	469	1046 ± 62	8.2 ± 0.5
$\overline{\Lambda}$	25	53 ± 22	0.4 ± 0.2
Σ^0 (‡)	22	76 ± 34	0.6 ± 0.3

(‡) The Σ^0 production rate has not been subtracted from the inclusive Λ production rate.

TABLE 7 : Mean values of kinematical variables for all charged current events (CC) and for charged current events containing K^0 mesons or Λ hyperons.
($p^\mu > 5$ GeV/c and $W^2 > (m_N + m_{K^0})^2$)

	CC Events	K^0 Events	Λ Events
E (GeV)	40.3 ± 0.3	50.2 ± 1.4	44.2 ± 1.5
ν (GeV)	12.5 ± 0.1	18.7 ± 0.7	16.0 ± 0.7
Q^2 (GeV^2)	4.62 ± 0.06	6.49 ± 0.31	5.55 ± 0.32
x	0.218 ± 0.001	0.210 ± 0.007	0.214 ± 0.007
y	0.315 ± 0.002	0.392 ± 0.009	0.353 ± 0.009
W^2 (GeV^2)	19.8 ± 0.2	29.5 ± 1.1	25.3 ± 1.2

TABLE 8 : Production properties of K^0 and Λ; p is the laboratory momentum.
($p^\mu > 5$ GeV/c and $W^2 > 5$ GeV^2)

	K^0	Λ
$< p >$ (GeV/c)	4.00 ± 0.19	2.69 ± 0.21
$< p_T^2 >$ (GeV/c)^2	0.26 ± 0.02	0.25 ± 0.02
p_T^2 slope (GeV/c)$^{-2}$	-4.93 ± 0.46	-4.69 ± 0.52
$< z >$	0.25 ± 0.01	0.22 ± 0.01
$< x_F >$	0.06 ± 0.01	-0.47 ± 0.02
$A = (N_F - N_B)/(N_F + N_B)$	0.23 ± 0.04	-0.72 ± 0.04
$< y^* >$	0.20 ± 0.03	-0.69 ± 0.03

TABLE 9 : Λ polarization along the x', y' and z' axes;
p is the laboratory momentum.
($p^\mu > 5$ GeV/c and $W^2 > (m_N + m_{K^0})^2$)

Selection cuts	$P_{x'}$	$P_{y'}$	$P_{z'}$
No cut	-0.56 ± 0.13	-0.02 ± 0.13	0.08 ± 0.13
$x_F < 0$	-0.63 ± 0.13	-0.02 ± 0.14	0.12 ± 0.14
$x_F > 0$	-0.11 ± 0.45	-0.06 ± 0.40	-0.01 ± 0.44
$p < 2$ GeV/c, $x_F < 0$	-0.57 ± 0.15	0.02 ± 0.16	0.02 ± 0.16
$p > 2$ GeV/c, $x_F < 0$	-0.82 ± 0.27	-0.24 ± 0.26	0.45 ± 0.27
$W^2 < 20$ GeV^2, $x_F < 0$	-0.60 ± 0.17	0.04 ± 0.19	0.18 ± 0.19
$W^2 > 20$ GeV^2, $x_F < 0$	-0.69 ± 0.21	-0.18 ± 0.22	0.00 ± 0.21
$Q^2 < 4$ GeV^2, $x_F < 0$	-0.61 ± 0.18	-0.01 ± 0.17	-0.05 ± 0.19
$Q^2 > 4$ GeV^2, $x_F < 0$	-0.64 ± 0.21	0.08 ± 0.24	0.39 ± 0.20
$x < 0.2$, $x_F < 0$	-0.46 ± 0.19	-0.01 ± 0.18	-0.20 ± 0.18
$x > 0.2$, $x_F < 0$	-0.85 ± 0.19	-0.02 ± 0.22	0.52 ± 0.20

FIGURE CAPTIONS

Fig. 1 Diagrams for dominant processes contributing to neutral strange particle production in antineutrino charged current interactions.

Fig. 2 Distribution of the cosine of the angle between the positive decay track and the V^0 line of flight (Lorentz boost direction) in the V^0 rest frame. (a) All K^0 fits before resolution of the ambiguities (the ambiguous V^0 are shown hatched); the dashed line represents the estimated contribution from true K^0 decays. (b) K^0 after resolution of the ambiguities (the contributions due to resolved ambiguities are shown hatched); (c) Λ as in (b).

Fig. 3 Distribution of unconstrained invariant mass; (a) $\pi^+\pi^-$ mass for K^0, (b) p π^- mass for Λ. The curves represent the fits described in the text.

Fig. 4 Lifetime distributions for (a) K^0_s, (b) Λ. The dashed lines do not represent fits to these distributions but were simply added to guide the eye. Their slopes are fixed by the average lifetimes determined by the maximun likelihood method.

Fig. 5 Invariant mass distribution for all $\Lambda\gamma$ combinations. The curve is the result of a polynomial fit to the background as described in the text.

Fig. 6 Average V^0 multiplicity as a function of the antineutrino energy E.

Fig. 7 Average V^0 multiplicity as a function of the energy transfer ν.

Fig. 8 Average V^0 multiplicity as a function of the 4-momentum transfer squared Q^2.

Fig. 9 Average V^0 multiplicity as a function of the Bjorken-x variable.

Fig. 10 Average V^0 multiplicity as a function of the Bjorken-y variable.

Fig. 11 Average V^0 multiplicity as a function of the hadronic invariant mass squared W^2 for (a) K^0 , (b) Λ . The data points for $\overline{\nu}$ n ($\times$) and $\overline{\nu}$ p (+) interactions extracted from reference 11 are also shown for comparison. The dashed curves are the predictions of the Lund model for deuterium taken from reference 11. Separate predictions for neutron and proton targets have been combined assuming $\sigma(\overline{\nu}\mathrm{p}) \simeq 2\sigma(\overline{\nu}\mathrm{n})$.

Fig. 12 Average V^0 multiplicity as a function of the hadronic invariant mass squared W^2; (a) K^0 in events with $Q = 0$. (b) K^0 in events with $Q = 1$. (c) Λ in events with $Q = 0$. (d) Λ in events with $Q = 1$. The curves are as in Fig. 11.

Fig. 13 Diagrams for Λ production in $\overline{\nu}$ interactions on a valence u quark off (a) a proton, (b) a neutron.

Fig. 14 Differential distribution of the V^0 transverse momentum squared with respect to the hadronic shower direction (normalized to the total number of charged current events). The solid lines are the result of the exponential fits described in the text whereas the dashed curves are as in Fig. 11.

Fig. 15 Differential distribution of the fraction of the W boson energy carried by the V^0 (normalized to the total number of charged current events). The curves are as in Fig. 11.

Fig. 16 Differential distribution of the Feynman-x variable (normalized to the total number of charged current events). The curves are as in Fig. 11.

Fig. 17 Differential distribution of the V^0 rapidity in the hadronic center of mass system (normalized to the total number of charged current events).

Fig. 18 Distribution of the cosine of the angle between the decay proton direction and (a) the x' axis (current direction), (b) the y' axis (perpendicular to the production plane), (c) the z' axis, in the Λ rest frame. The lines represent the results of the fits described in the text.

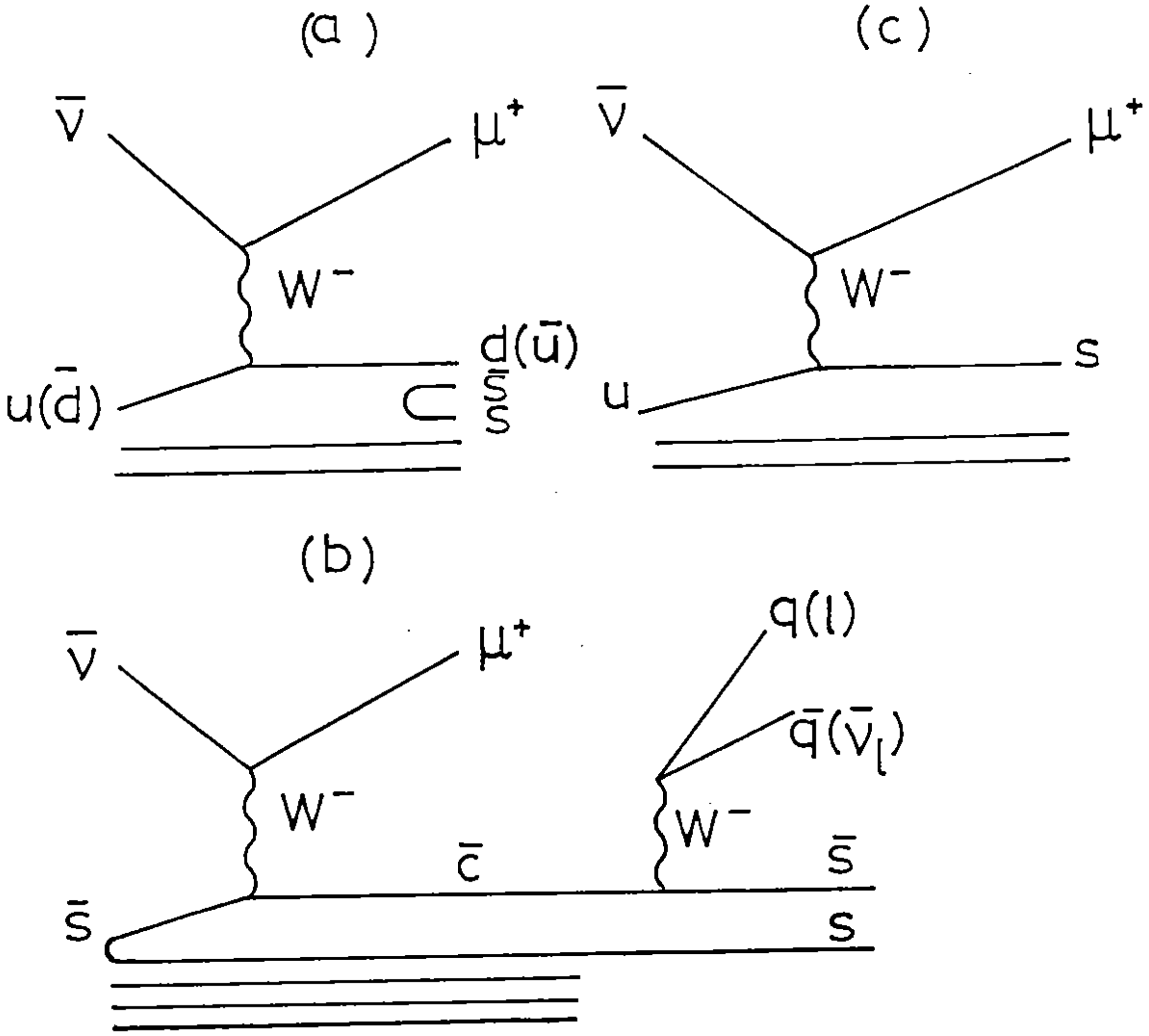(a)
$\bar{\nu}$
μ^+
W^-
$d(\bar{u})$
$u(\bar{d})$
$\subset$
$\bar{s}$
s
(c)
$\bar{\nu}$
μ^+
W^-
s
u
(b)
$\bar{\nu}$
μ^+
$q(l)$
$\bar{q}(\bar{\nu}_l)$
W^-
W^-
$\bar{c}$
$\bar{s}$
$\bar{s}$
s

FIG.1

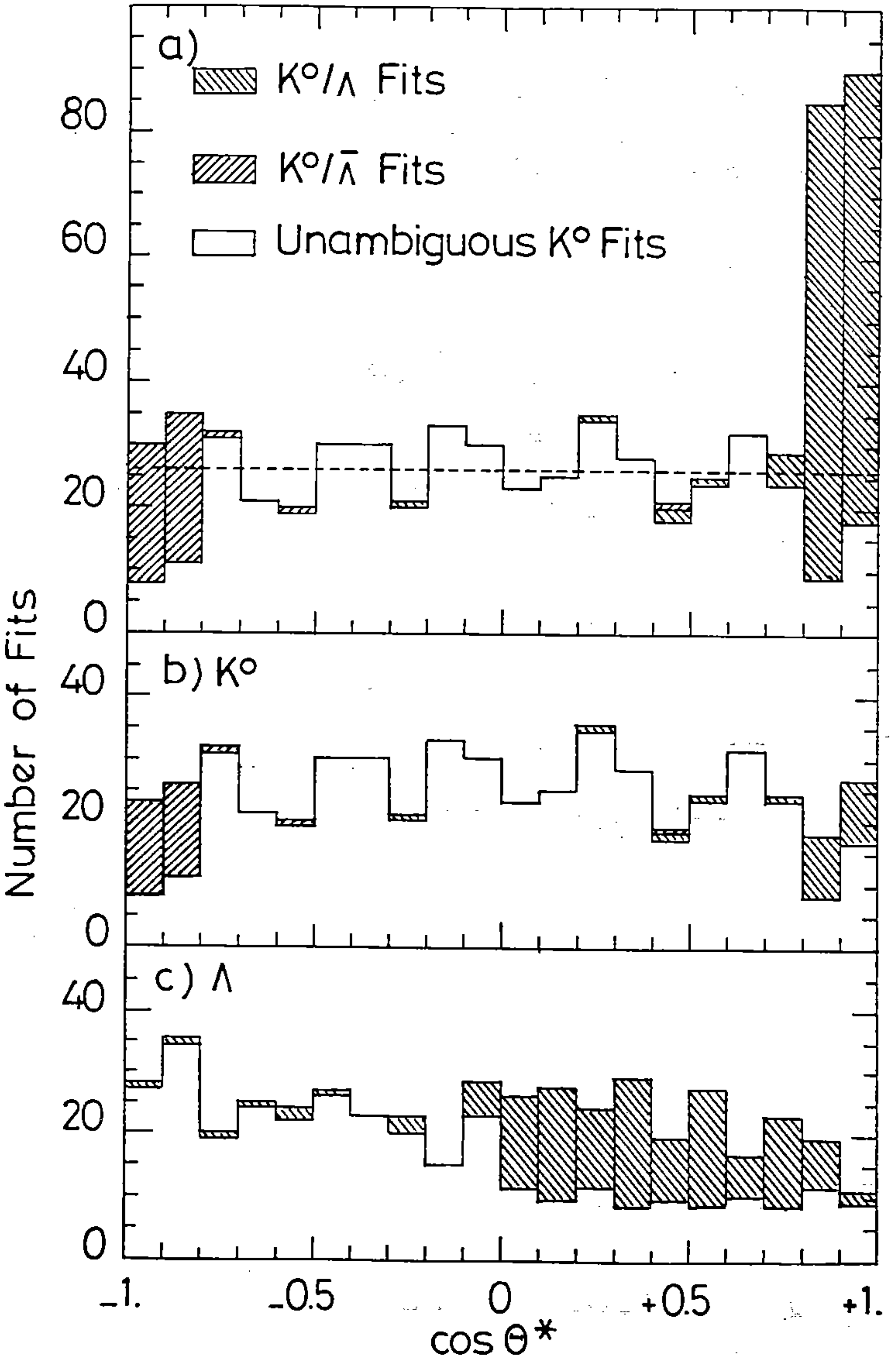
a)
K°/Λ Fits
K°/Λ̄ Fits
Unambiguous K° Fits
b) K°
c) Λ
Number of Fits
0
20
40
60
80
-1.
-0.5
0
+0.5
+1.
cos Θ*

FIG. 2

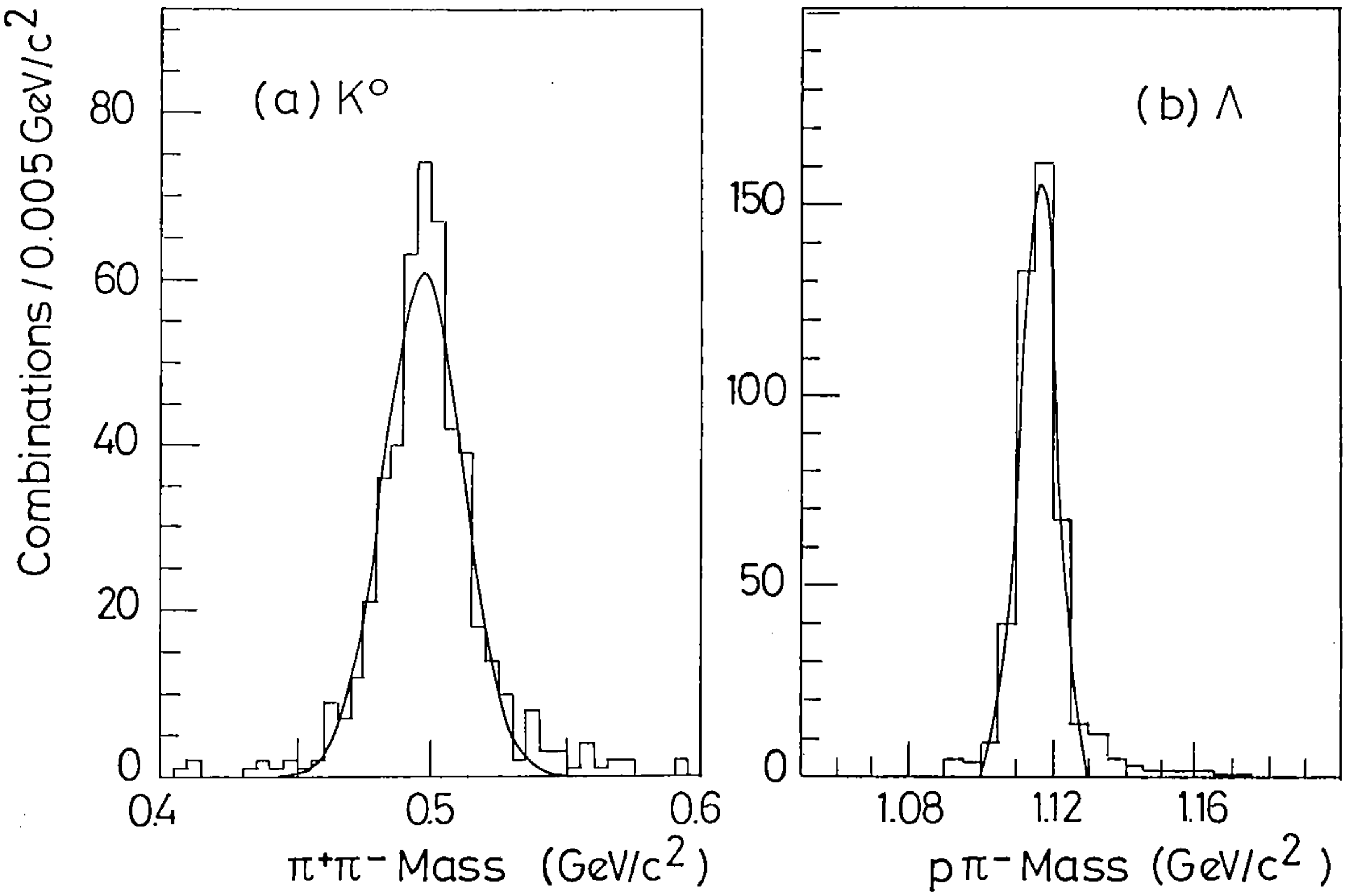
Combinations / 0.005 GeV/c^2
(a) K^o
80
60
40
20
0
0.4
0.5
0.6
$\pi^+\pi^-$ - Mass (GeV/c^2)
(b) Λ
150
100
50
0
1.08
1.12
1.16
$p\pi^-$ - Mass (GeV/c^2)

FIG. 3

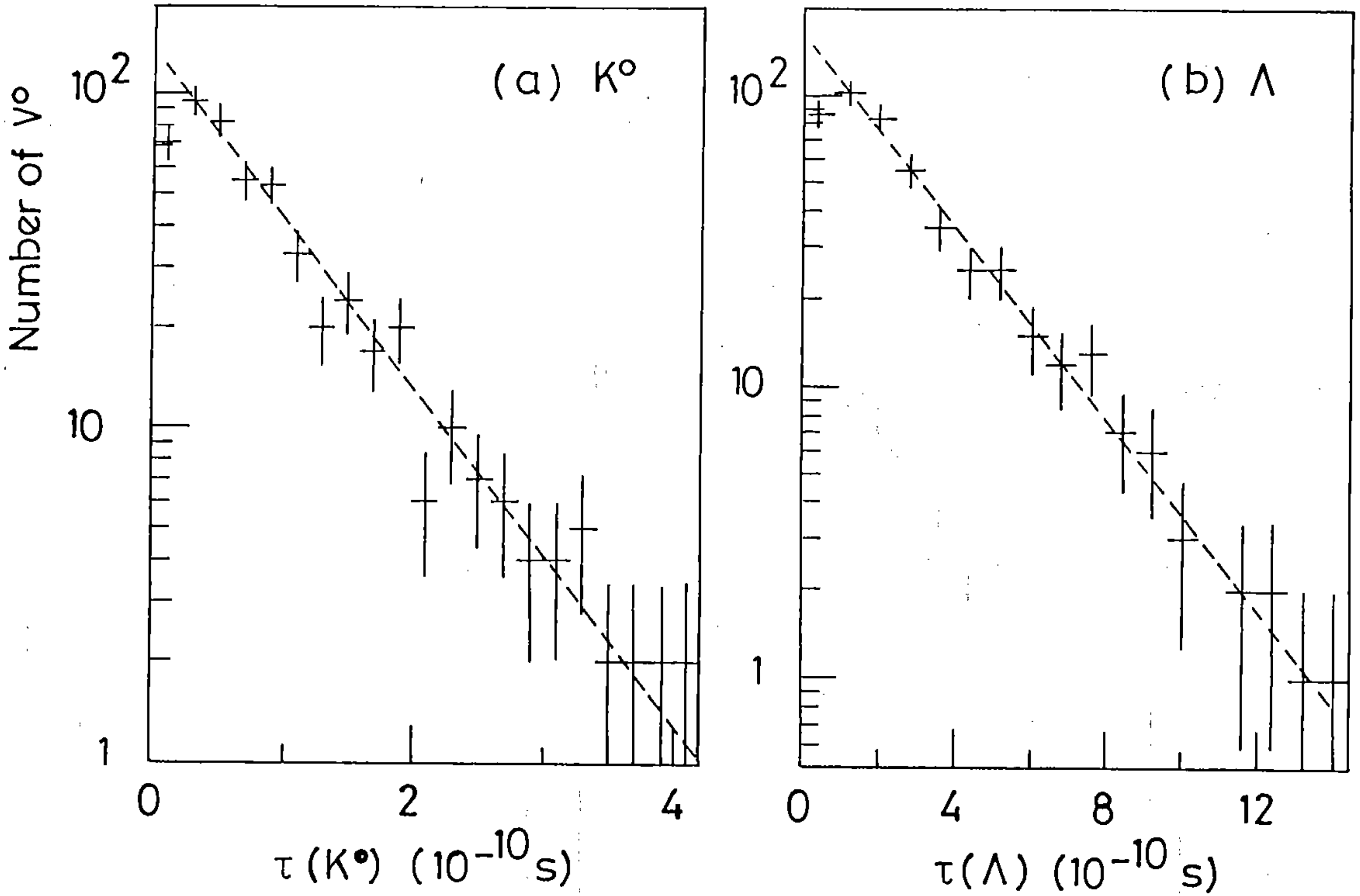

FIG.4

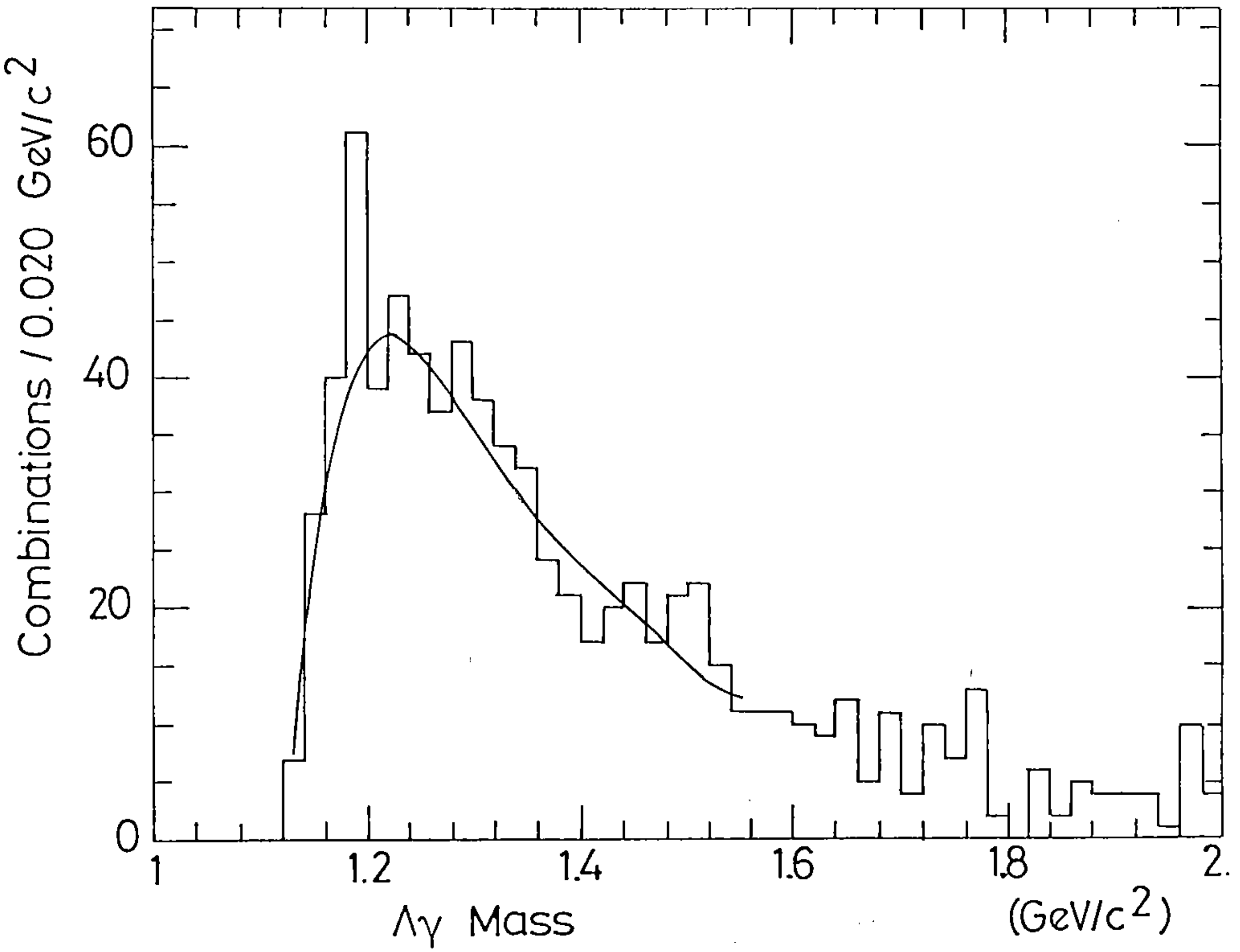

FIG. 5

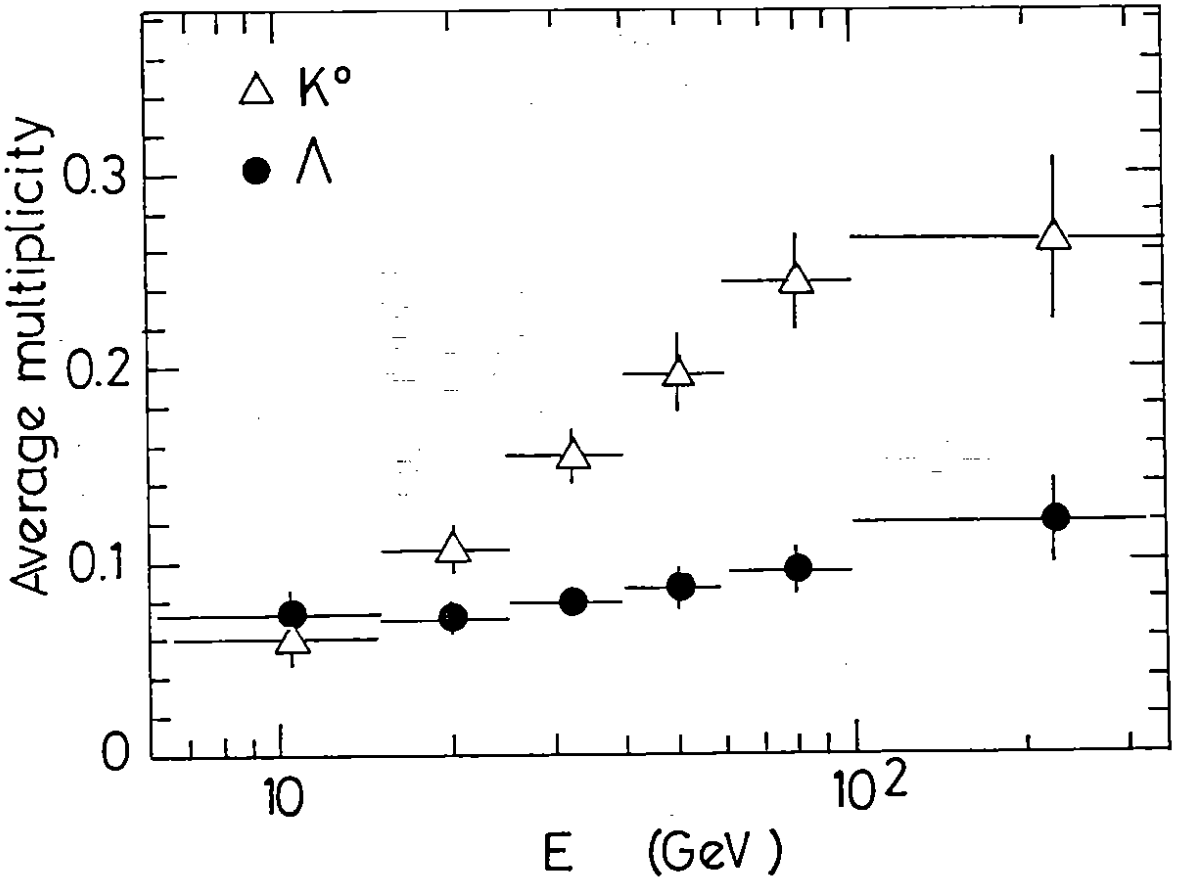

FIG. 6

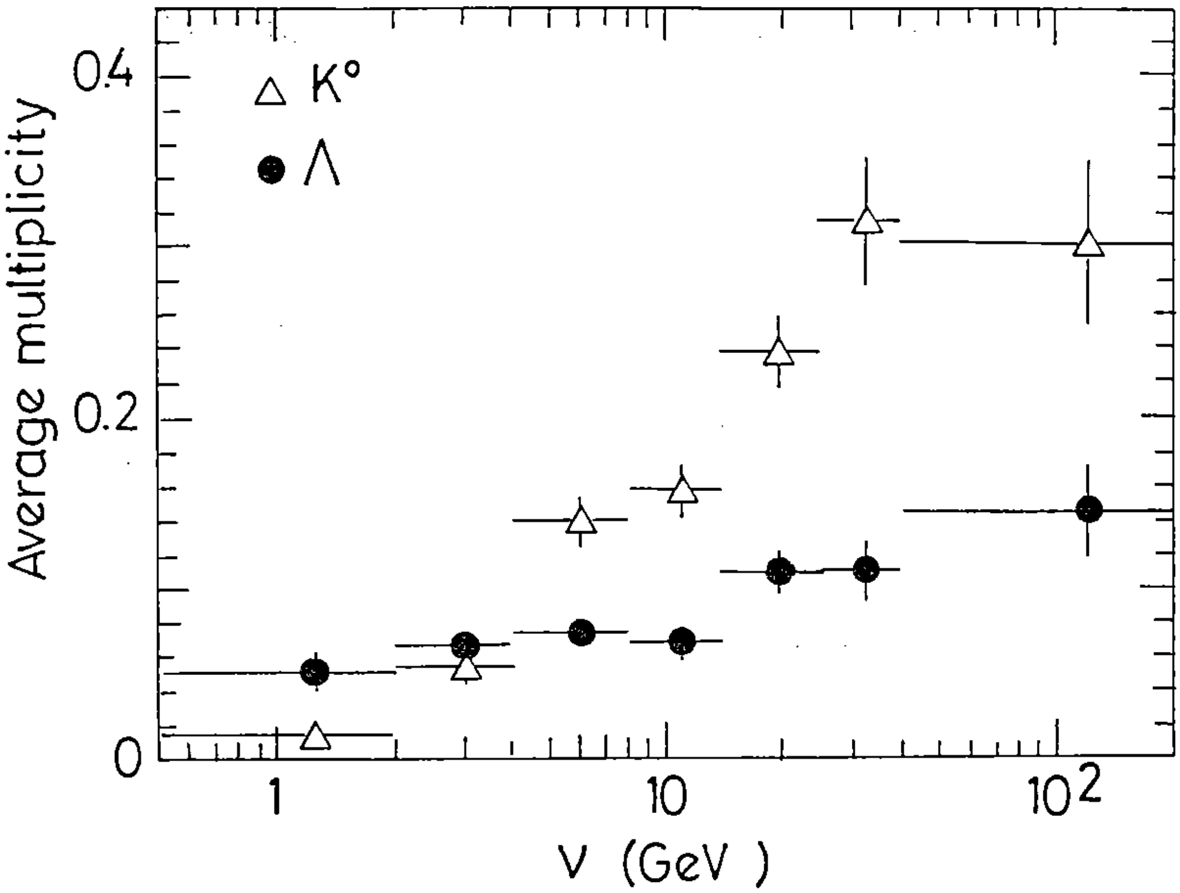

FIG. 7

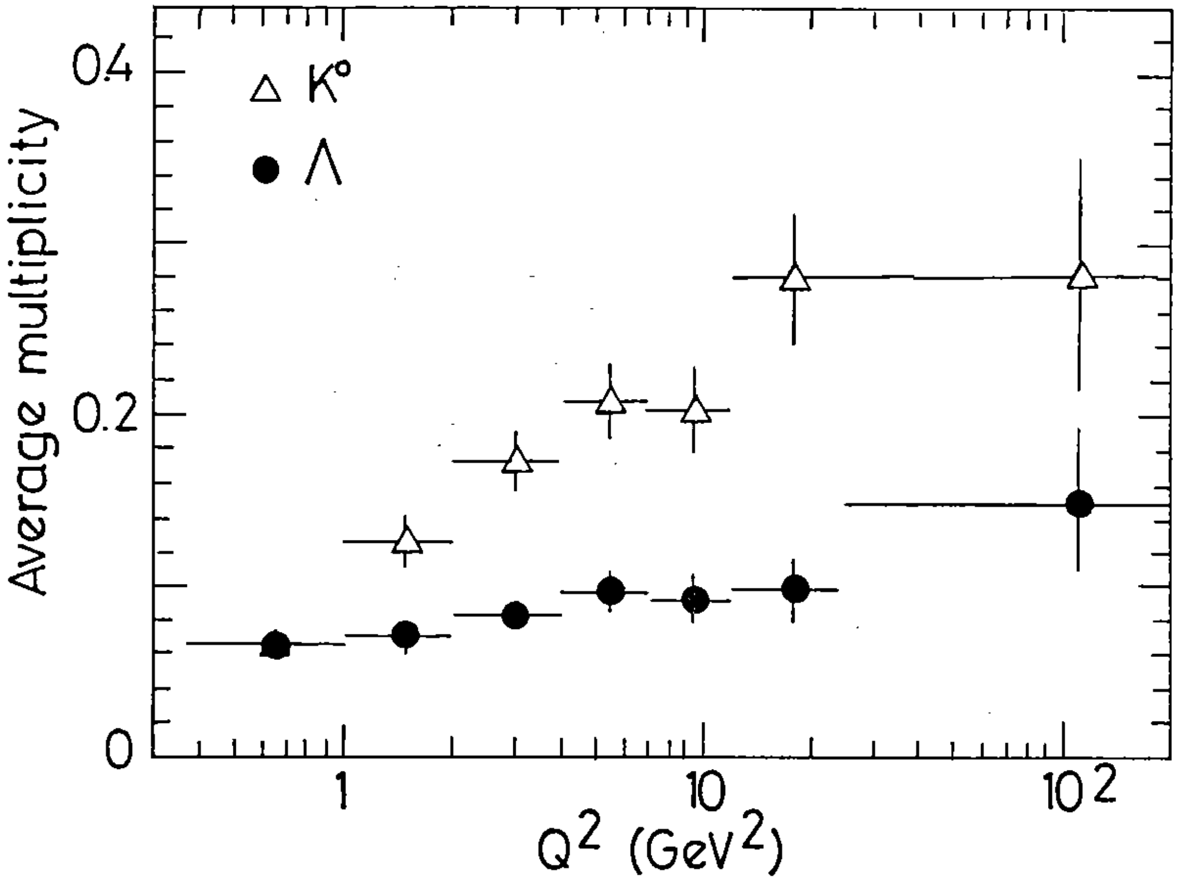

FIG.8

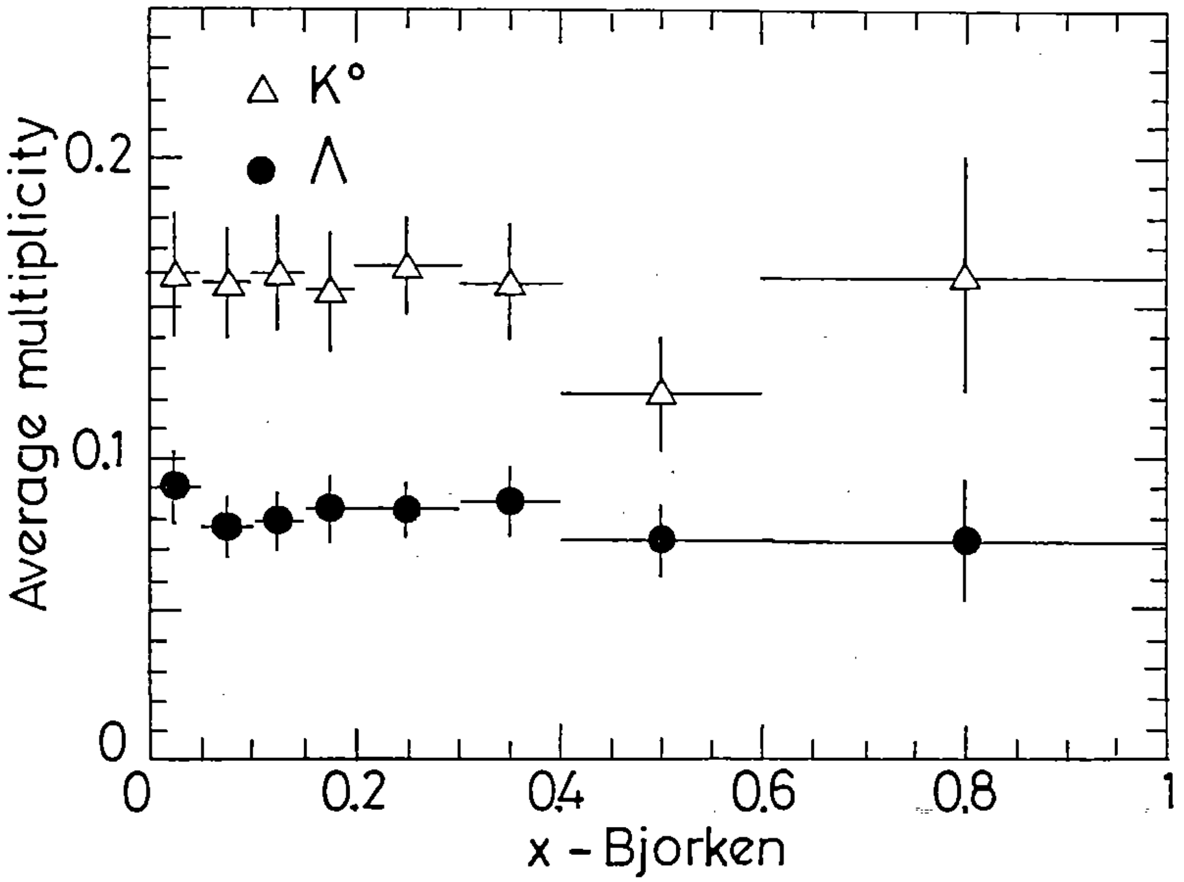

FIG. 9

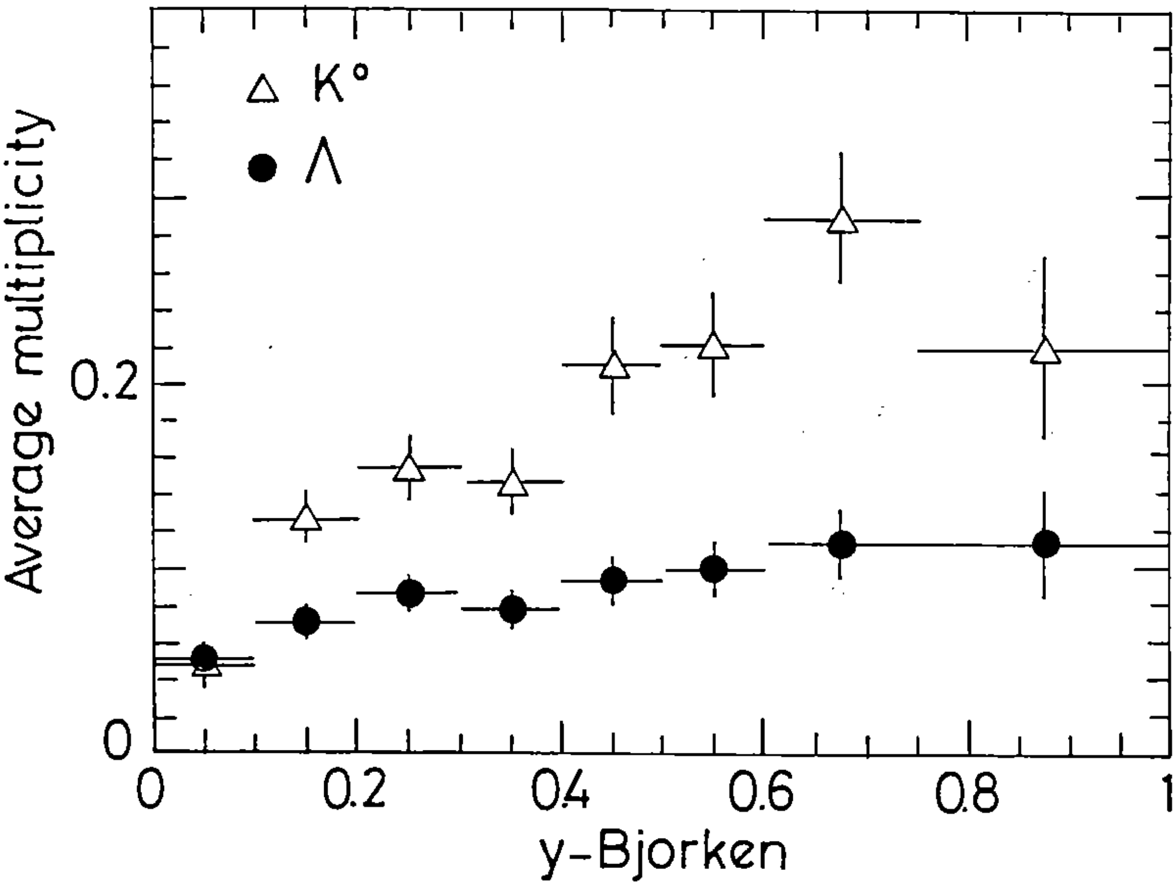

FIG.10

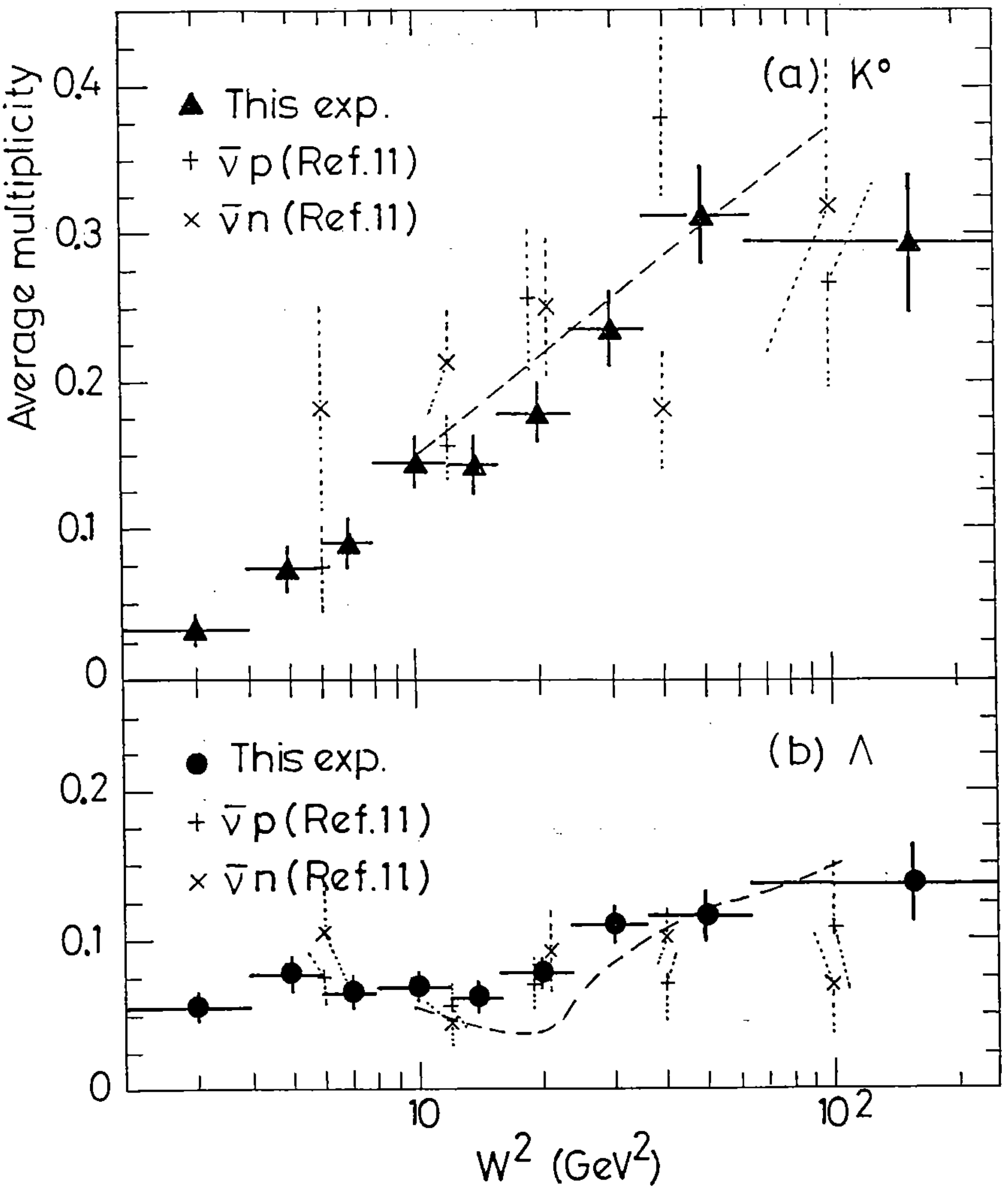

Average multiplicity
0.4
0.3
0.2
0.1
0
▲ This exp.
+ $\bar{\nu}$p (Ref.11)
× $\bar{\nu}$n (Ref.11)
(a) K°
0.2
0.1
0
● This exp.
+ $\bar{\nu}$p (Ref.11)
× $\bar{\nu}$n (Ref.11)
(b) Λ
10
10^2
W^2 (GeV^2)

FIG.11

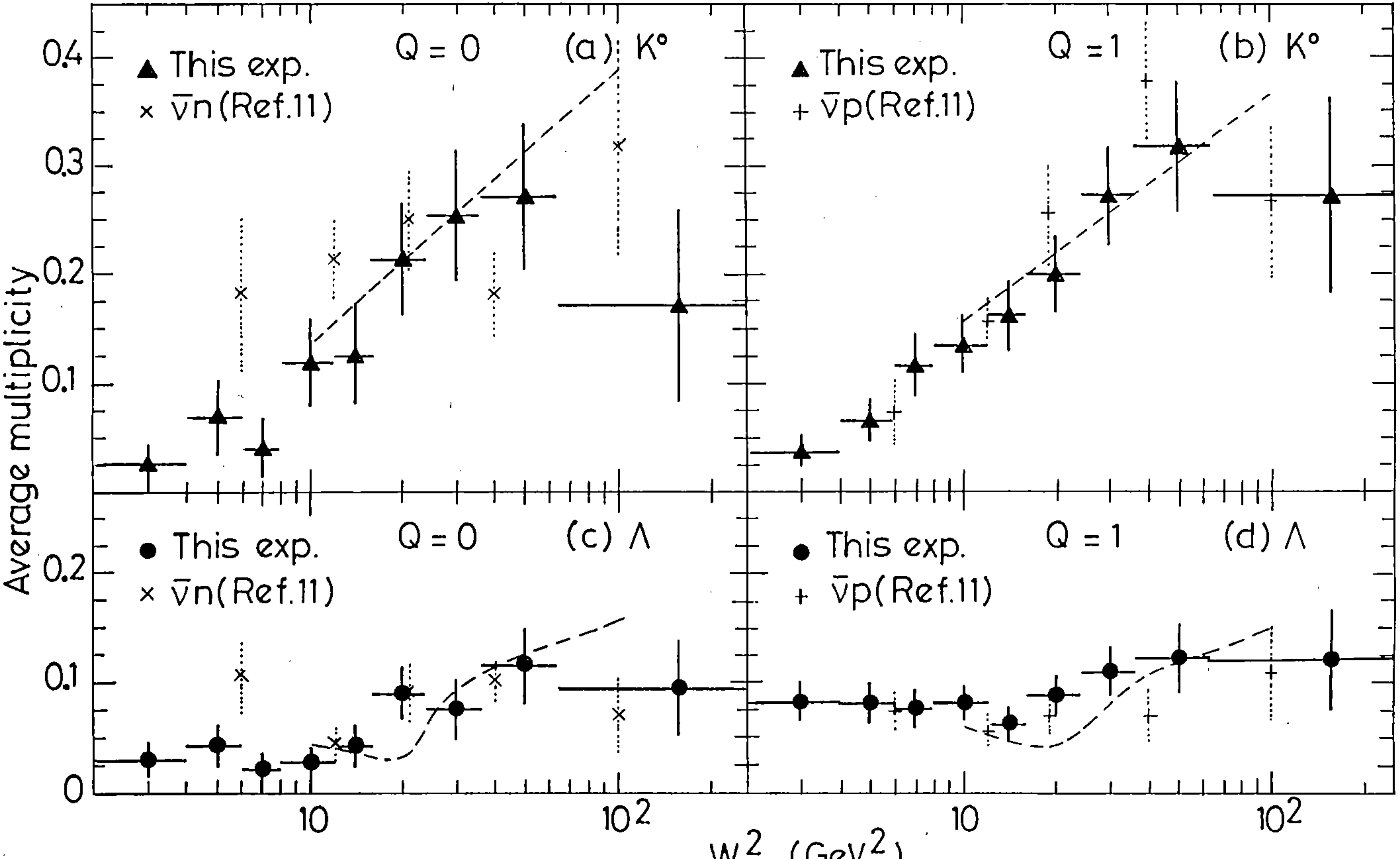
Average multiplicity
0.4
0.3
0.2
0.1
0
Q = 0
(a) K°
▲ This exp.
× $\bar{\nu}$n(Ref.11)
Q = 1
(b) K°
▲ This exp.
+ $\bar{\nu}$p(Ref.11)
Q = 0
(c) Λ
● This exp.
× $\bar{\nu}$n(Ref.11)
Q = 1
(d) Λ
● This exp.
+ $\bar{\nu}$p(Ref.11)
10
10^2
10
10^2
W^2 (GeV^2)

FIG.12

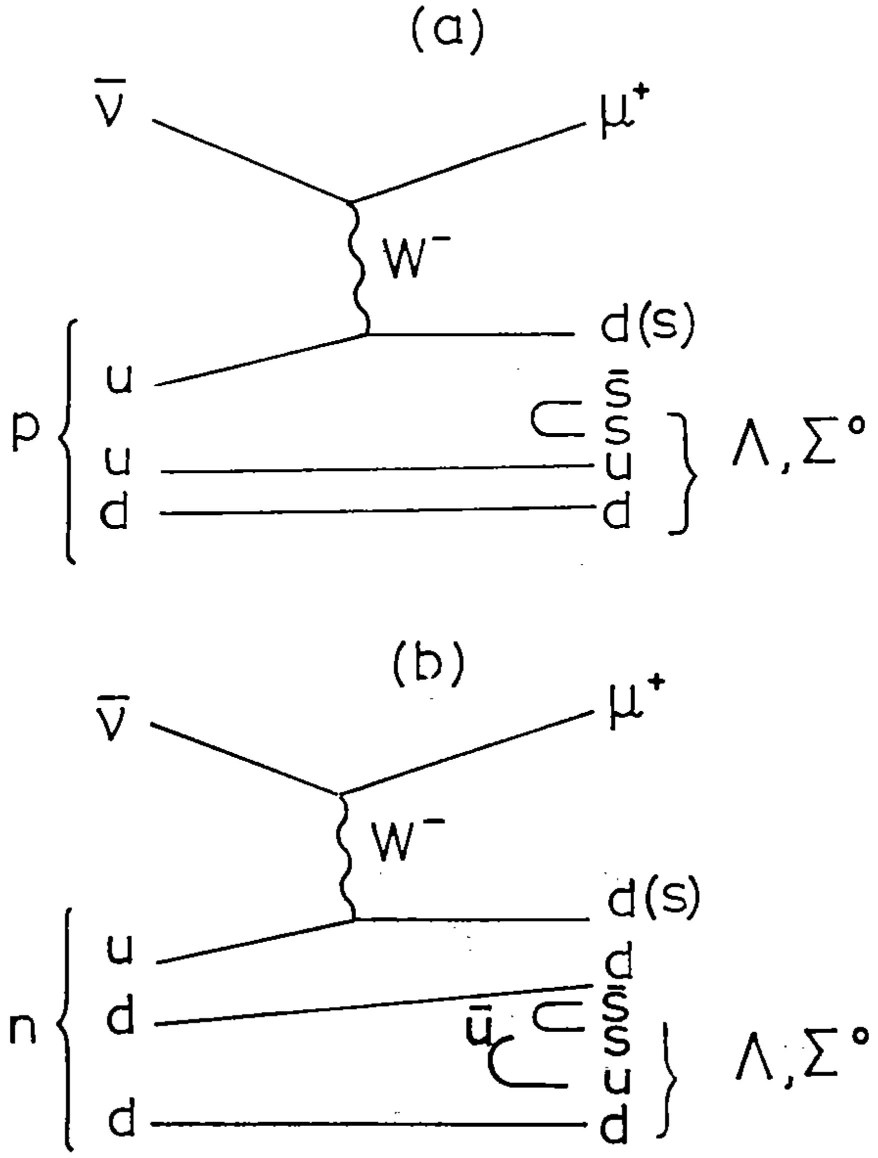
(a)
$\bar{\nu}$
μ^+
W^-
d(s)
p
u
u
d
$\bar{s}$
s
u
d
Λ, Σ^0
(b)
$\bar{\nu}$
μ^+
W^-
d(s)
n
u
d
d
d
$\bar{u}$
$\bar{s}$
s
u
d
Λ, Σ^0

FIG.13

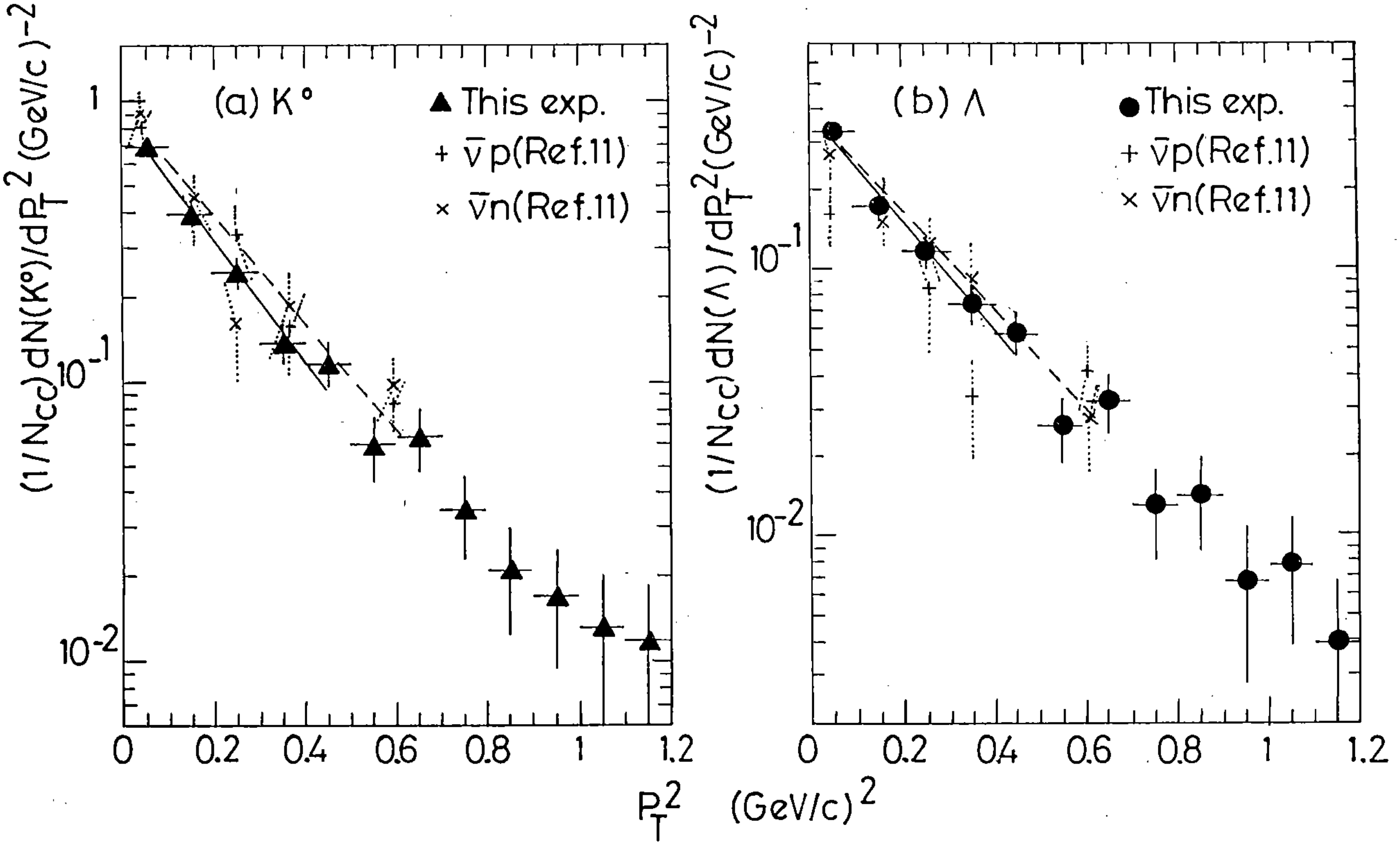
(1/N$_{cc}$) dN(K°)/dP$_T^2$ (GeV/c)$^{-2}$
1
10^{-1}
10^{-2}
(a) K°
▲ This exp.
+ $\bar{\nu}$p(Ref.11)
× $\bar{\nu}$n(Ref.11)
(1/N$_{cc}$) dN(Λ) / dP$_T^2$(GeV/c)$^{-2}$
10^{-1}
10^{-2}
(b) Λ
● This exp.
+ $\bar{\nu}$p(Ref.11)
× $\bar{\nu}$n(Ref.11)
0
0.2
0.4
0.6
0.8
1
1.2
P$_T^2$ (GeV/c)^2

FIG. 14

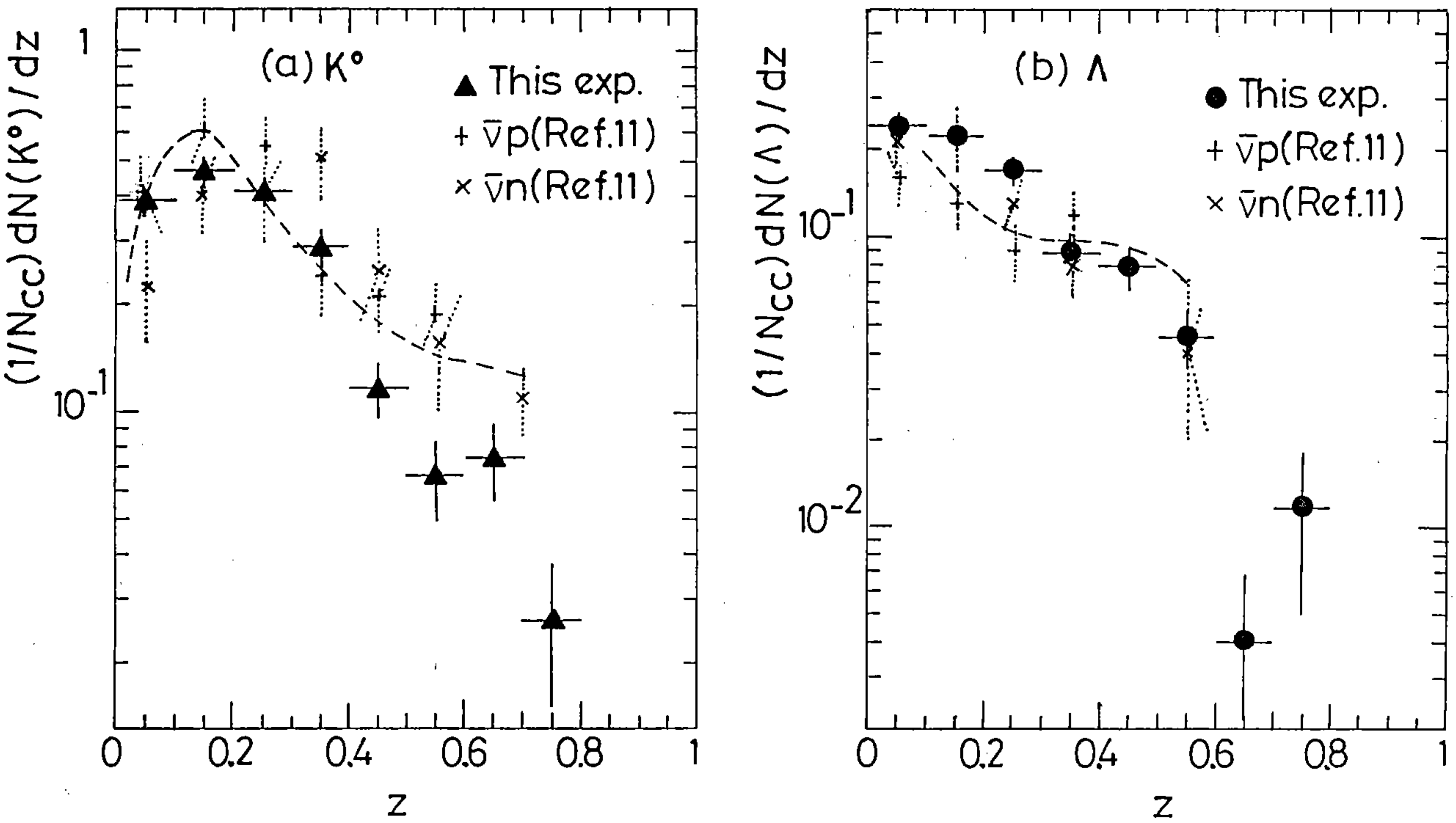
(a) K°
▲ This exp.
+ $\bar{\nu}p$(Ref.11)
× $\bar{\nu}n$(Ref.11)
(1/N_cc) dN(K°) / dz
1
10^{-1}
0
0.2
0.4
0.6
0.8
1
z
(b) Λ
● This exp.
+ $\bar{\nu}p$(Ref.11)
× $\bar{\nu}n$(Ref.11)
(1/N_cc) dN(Λ) / dz
10^{-1}
10^{-2}
0
0.2
0.4
0.6
0.8
1
z

FIG.15

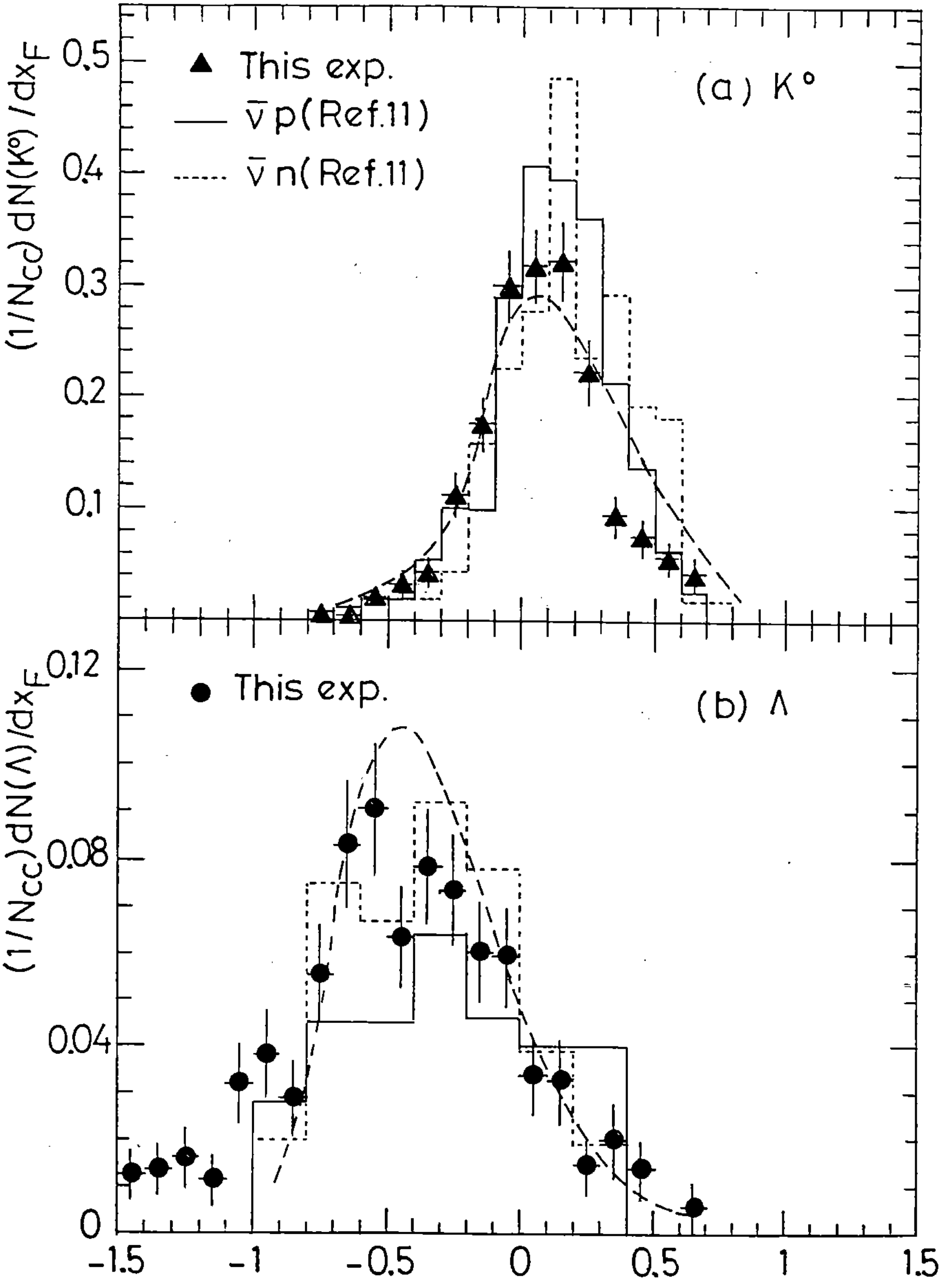
▲ This exp.
— ν̄p(Ref.11)
----- ν̄n(Ref.11)
(a) K°
(1/N_cc) dN(K°) /dx_F
0.5
0.4
0.3
0.2
0.1
● This exp.
(b) Λ
(1/N_cc) dN(Λ)/dx_F
0.12
0.08
0.04
0
-1.5
-1
-0.5
0
0.5
1
1.5
x- Feynman

FIG. 16

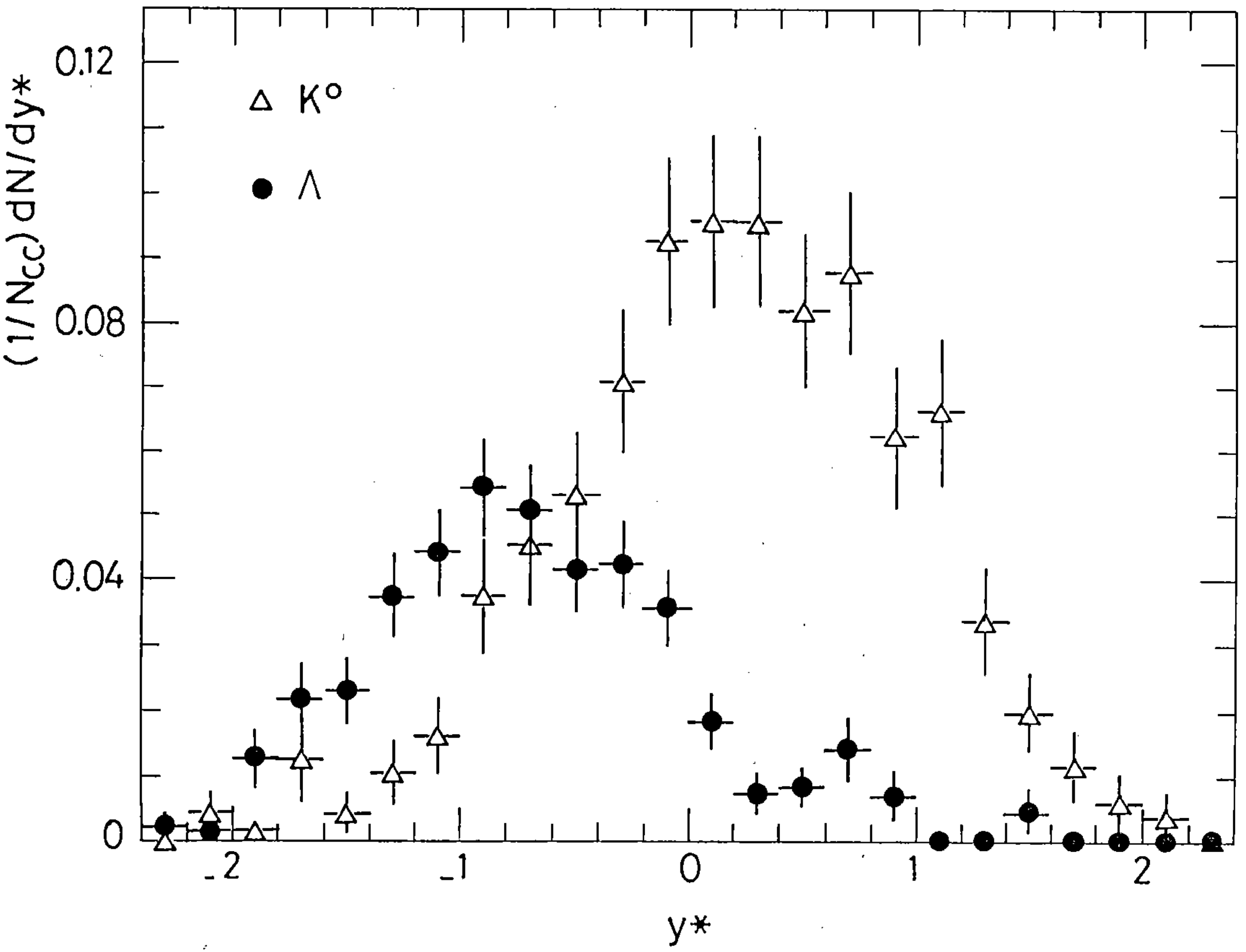

FIG.17

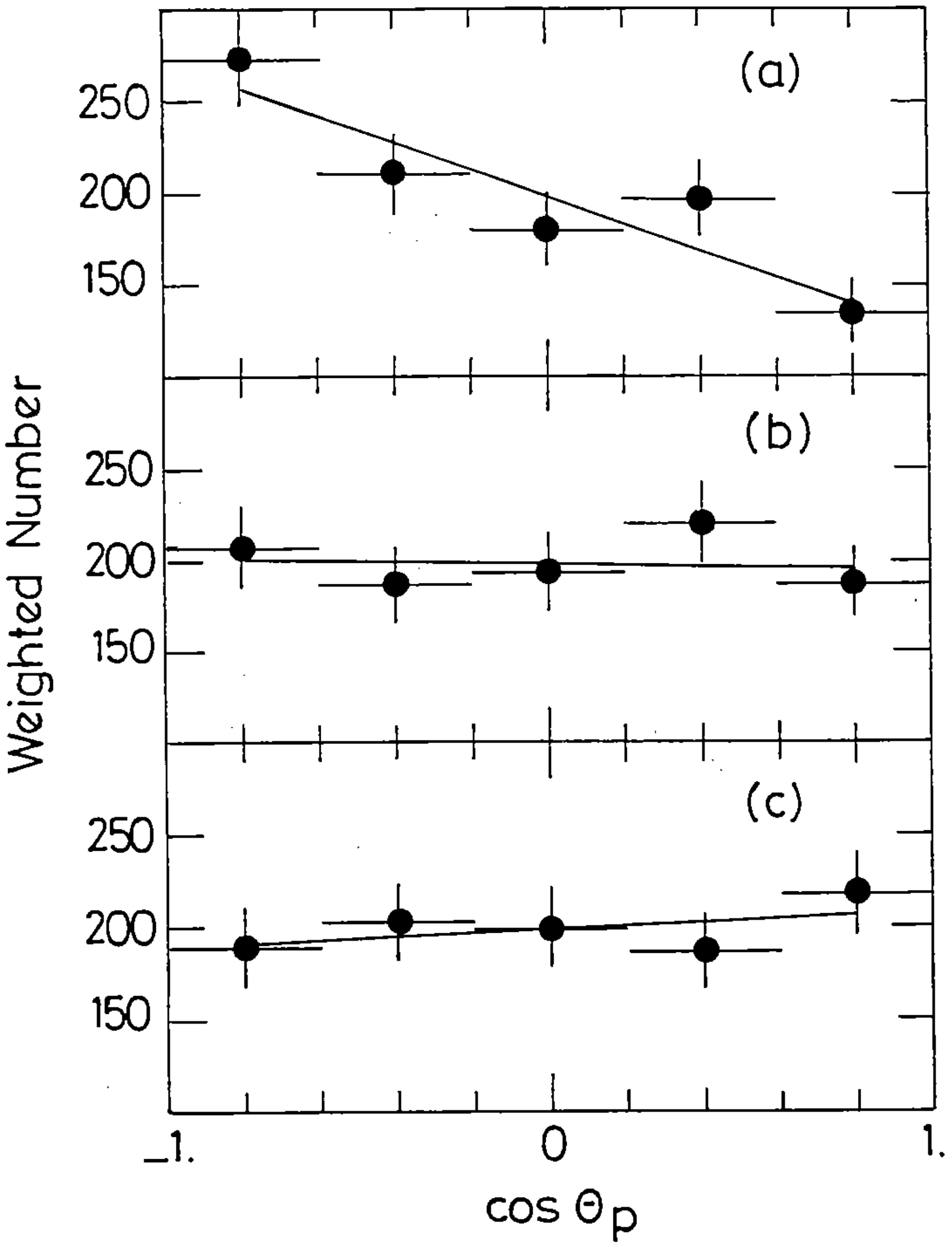

FIG.18